Investigations on the Performance of Grounding Device with Spike Rods (GDSR) with the Effects of Soil Resistivity and Configurations

Abdul Wali Abdul Ali [1], **Nurul Nadia Ahmad** [1], **Normiza Mohamad Nor** [1,*] , **Nur Farahi Idris** [1] **and Farhan Hanaffi** [2]

[1] Faculty of Engineering, Multimedia University, Jalan Multimedia, Cyberjaya 63100, Malaysia; walikdr17@gmail.com (A.W.A.A.); nurulnadia.ahmad@mmu.edu.my (N.N.A.); nurfarahi.idris@gmail.com (N.F.I.)

[2] Faculty of Electrical Engineering, Universiti Teknikal Malaysia Melaka (UTeM), Melaka 76100, Malaysia; farhan@utem.edu.my

[*] Correspondence: normiza.nor@mmu.edu.my

check for updates

Abstract: In a recently published work, the characteristics of a new grounding device with spike rods (GDSR) with various arrangements of ground electrodes under high magnitude impulse currents (up to 16 kA), was investigated. In an earlier study, the ground electrodes were installed in low resistivity test media, with resistance at steady state (Rdc) values ranging from $11\,\Omega$ to $75\,\Omega$. In practice, various soil resistivity, ranging from a few Ohm-metres to several kiloOhm-metres, have been reported in the standards. It is, therefore, necessary to investigate the characteristics of GDSR with different arrangements of ground electrodes in various soil resistivities under high impulse currents. In this present paper, six configurations of ground electrodes are used, installed at three different sites and subjected to high impulse conditions. Impulse test data of all the grounding systems are analyzed. The Finite Element Method (FEM) is used to compute the electric field values of the ground electrodes achieved. It is found that the highest electric field occurs in the presence of electrodes with the highest Rdc, soil resistivity and current magnitudes. This new data would be useful in bolstering the performance of GDSR in various types of soil resistivities, electrode arrangements and current magnitudes, which may allow for optimum design of grounding systems.

Keywords: earthing systems; electrode geometry; fast-impulses; high-magnitude currents

1. Introduction

There are two main parameters that affect the design of grounding systems; ground electrode configurations and soil resistivity. A few standards [1–4] list useful formulae for the computation of resistance at steady state (Rdc), Ground Potential Rise (GPR), Touch Voltage (VT) and Step Voltage (Vs). These standards [2–5] also include soil resistivity data, which varies over several orders of magnitudes to thousands of ohm-metres. It is important to highlight that this information deals with the grounding system performance at low voltage, which is usually different for the case of practical grounding system applications under high impulse conditions.

Many publications reported investigations on the practical grounding system by field measurements under high impulse conditions, where the grounding systems consist of a few electrodes, as used in [5–8], counterpoises [9–11] and full-scale grounding grids [12–14]. All of these studies [6–14] show that the behavior of the ground electrode is different from the low voltage, low frequency current, where three conditions would happen when practical grounding systems are subjected to high impulse current; (a) reduction of impulse ground resistance value with increasing currents,

(b) current-independent of ground resistance value for some electrodes, and (c) higher impulse resistance value than Rdc [14].

Haddad et al. [9] reported the results of impulse characteristics of practical ground electrodes consisting of isolated tower legs (Leg 1, 2 3 and 4), full-scale tower base (RT) and the ring electrode (Ro). The DC resistance was the highest for Leg 1 (108.2 Ω), followed by Leg 3 (75.8 Ω), Leg 2 (64.6 Ω), Leg 4 (55.3 Ω), RT (18.5 Ω) and Ro (1.8 Ω). They [11] found that when the current increased from 600 A to 6 kA, the impulse resistances decreased by 47% for Leg 1, 40% for Leg 3, 22% for Leg 2 and 14% for Leg 4. They [9] noted that soil ionisation is more likely to occur with electrodes of small surface area and high soil resistivity (high Rdc) and high impulse currents. Similarly, Ali et al. [5] and Reffin et al. [7] observed that for some grounding systems, the higher the Rdc, the higher the impulse resistance reduction is, demonstrating strong current-dependent characteristics. On the other hand, Stojkovic et al. [14] discovered that under transients, the impulse impedance was higher, compared to the steady-state resistance, Rdc. They [14] described an increase of impulse impedance from its steady state values due to the influence of the large grounding grid configuration and its length. However, for the large grounding electrodes, 50 m × 52.5 m, and 0.8 m deep, Yang et al. [12] reported a reduction in impulse grounding resistance with increasing currents for different response times and injection points. All of these studies [5–14] showed that there are a few factors contributing to the impulse characteristics of grounding systems.

These also include the soil resistivity values, which are significantly affected by moisture content, temperature, types of soil, soil grain size and a variation in the thickness of soil layers from one site to another. Despite much research work [5–14] published on the impulse characteristics of grounding systems for different soil resistivities, the measurements are still important due to many variations in soil. Elzowawi et al. [15] performed a series of tests, having a two-layer soil model with various thicknesses and percentages of water content for both layers. They [16] found that differences in soil resistivity affect the impulse characteristics of grounding systems. This, in turn, can affect the ground potential rise (GPR), touch and step voltages. This shows that it is important to include soil resistivity values correlating with impulse characteristics of grounding systems. Further, it has been proven that the soil resistivity and permittivity affects the response of grounding electrodes subjected to lightning currents, and at various frequencies [16–19]. These studies [16–19] found that soil resistivity, hence impulse impedance, starts to increase at certain frequencies, depending on soil resistivity value. For low soil resistivity, an increase in impulse impedance starts at low frequency values, while for high soil resistivity, higher frequency values cause an increase in impulse impedance. This shows that the impulse characteristics of grounding systems depend strongly on the electrical properties of soil.

In this present paper, six grounding electrodes are tested under impulse conditions, and the results are analysed. The soil resistivity of each site and the Rdc of grounding electrodes are measured in order to predict the type of soil most suitable for GDSR and electrode arrangement. These ground electrodes are tested under various magnitudes of current, which provide information about the suitability of these ground electrodes to be used for low or high voltage system levels. Further, this will help power engineers to design earth electrodes, with consideration of the ionization process in soil. Electric field distribution is also computed using Finite Element Method (FEM) software for all the electrodes installed in different soil media.

2. Experimental Arrangement

In previously published work [5], various ground electrodes were installed in low resistivity soil. In this paper, similar arrangements of ground electrodes, as in Ref. [5] are used and installed in four sites, including the site previously published in work [5]. All these six configurations, with their dimensions, are summarized in Table 1. The soil resistivity of each test site is first measured using the Wenner method. The measured soil resistivity data is then processed into the RESAP module of Current Distribution, Electromagnetic Fields, Grounding and Soil Structure Analysis (CDEGS) [20], which is interpreted into 2-layer soil model. Table 2 summarizes the computed resistivity data for all

locations. Soil resistivity data for site 3 is obtained from Ref. [5], which has the lowest soil resistivity among all three sites.

Table 1. Details of grounding systems configurations used in the study

Configurations of Grounding Systems	
Configuration 1	Configuration 4
Configuration 2	Configuration 5
Configuration 3	Configuration 6
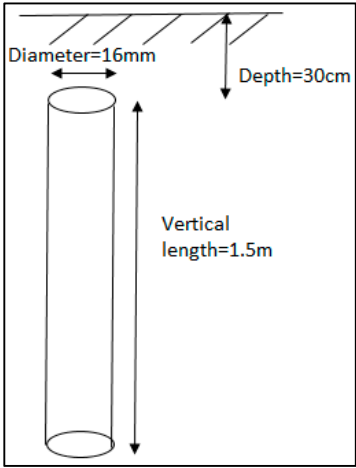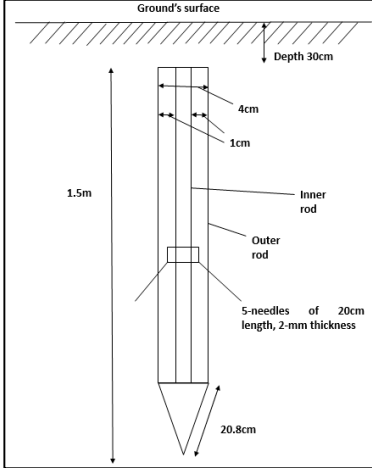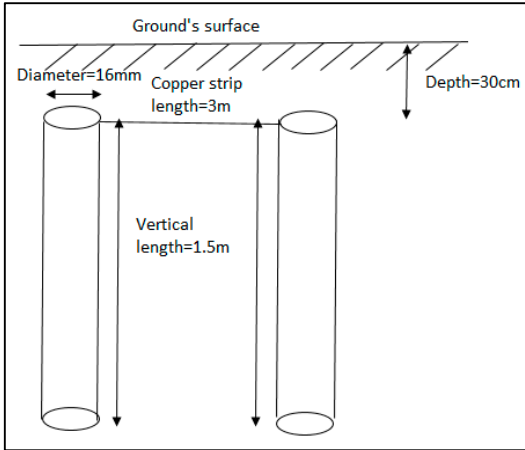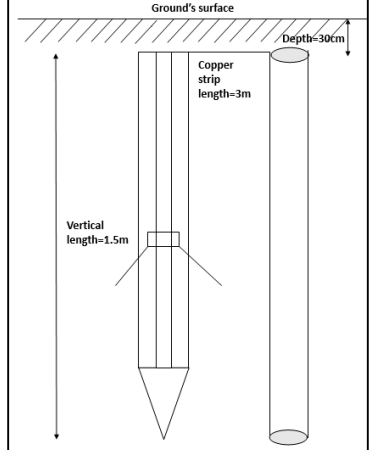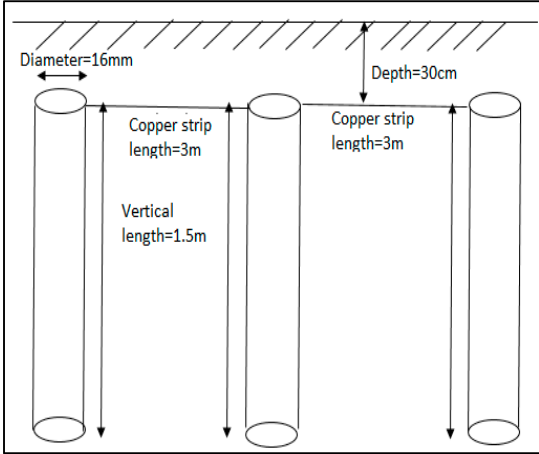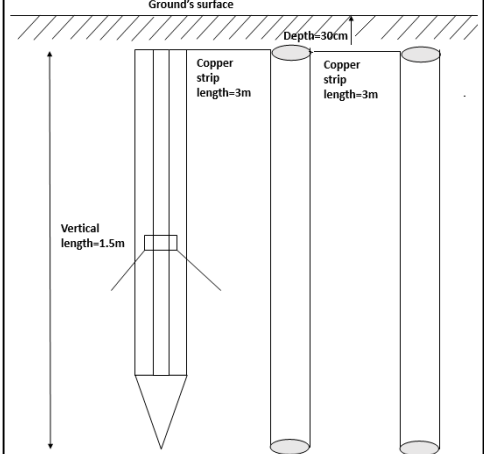
Table 2. Computed 2-layer soil resistivity model at different locations.

Location	ρ_1 ($\Omega\cdot m^{-1}$)	h_1 (m)	ρ_2 ($\Omega\cdot m^{-1}$)	h_2 (m)
Site 1	57.2	6.0	758.1	∞
Site 2	160.4	4.3	359.6	∞
Site 3	3	4.9	0.2	∞

The Rdc measurements are carried out using the Fall-of-Potential (FoP) method. The results of the measured Rdc for different configurations in various soil resistivity are presented in Table 3. As is expected, ground electrodes at site 2 have the highest measured RDC because of their relatively high resistivity. It was noticed that all the rods are buried within the depth of the upper layer of soil resistivity, ρ_1, thus, a ratio of ρ_1 to the Rdc is taken, and summarized in Table 4. As can be seen in Table 4, the highest ratios are seen for site 2, with the highest ρ_1, followed by site 1 and site 3. However, when comparisons between conf. 1 and conf. 4, conf. 2 and conf. 5, conf. 3 and conf. 6 are made, the highest percentage is seen for site 3 (with the lowest soil resistivity), followed by site 2 and 1. This can be an indication that GDSR can reduce the Rdc more significantly than conventional electrodes in low resistivity soil.

Table 3. Measured resistance at steady state (Rdc) for all configurations at different locations.

Conf.	Earth Electrode	Rdc (Ω) of Ground Electrodes		
		Site 1	Site 2	Site 3
1	A vertical single rod electrode	67.02	104.4	75.52
2	2 parallel vertical rod electrodes	25.02	44.8	27.56
3	3 parallel vertical rod electrodes	16.6	28.5	17.81
4	GDSR	53.0	67.2	18.5
5	GDSR in parallel with vertical one rod electrode	23.4	37.6	14.6
6	GDSR with spike rods in parallel with two vertical rods	16.21	26.6	11.33

Table 4. Ratio of upper layer of soil resistivity, ρ_1 to Rdc.

Conf.	Earth Electrode	Rdc (Ω) of Ground Electrodes		
		Site 1	Site 2	Site 3
1	A vertical single rod electrode	0.85	1.54	0.04
2	2 parallel vertical rod electrodes	2.28	3.58	0.11
3	3 parallel vertical rod electrodes	3.44	5.63	0.17
4	GDSR	1.08	2.39	0.16
5	GDSR in parallel with vertical one rod electrode	2.44	4.27	0.21
6	GDSR with spike rods in parallel with two vertical rods	3.53	6.03	0.26

In this work, a similar configuration of remote earth, as demonstrated in previous work [5] is used, but this time, installed at all three locations. Using a Fall-of-Potential (FOP) method, Rdc for remote earth installed at sites 1, 2 and 3, and are found to be 8.8 Ω, 16.8 Ω and 4.8 Ω, respectively. All of these ground resistance values of remote earth are lower than the electrodes under test. This complies with the IEEE Standard 81 [4], in which the earth resistance of remote earth should be lower than the electrode under test when performing impulse tests on grounding systems. For site 3, the test circuit and arrangement are placed as in previously published work [5], with the impulse generator capable of generating high voltages up to 1200 kV and high current impulses up to 30 kA. On the other hand, for sites 1 and 2, a similar test arrangement and test circuit are applied as in previous work [9,10],

with a smaller impulse generator, capable of generating high voltages up to 300 kV and high current impulses up to 10 kA. The impulse generator used for testing electrodes at site 3, has 6 stages; each stage can generate up to 200 kV, and a capacitance per stage of 1 μF, while the impulse generator used for testing electrodes at sites 1 and 2 consists of 3 stages, with each stage capable of generating up to 100 kV, with the capacitance per stage of 2 μF.

Figure 1 shows the test arrangement adopted in this study, which is similar to the filed patent [21], and used in References [5,7,8]. In this arrangement, a diesel generator is used to feed the power to the impulse generator, using a power cable, 1. The grounded terminal of the impulse generator is grounded to the remote earth, where its Rdc is lower than the Rdc of grounding systems under tests, with the meshed copper wires, 2. The live terminal of the impulse generator is connected to the grounding system under tests, where these copper mesh wires go through a current transformer for current measurements. The same connection goes to the grounding system under tests, branched out to a resistive divider, with the meshed copper wires, 2, for voltage measurements. This potential divider is grounded with a single rod electrode. Two separate units of Digital Storage Oscilloscopes (DSOs) are used to capture the voltage and current signals separately. Coaxial cables, 3, are connected to the current transformer and resistive divider of these DSOs.
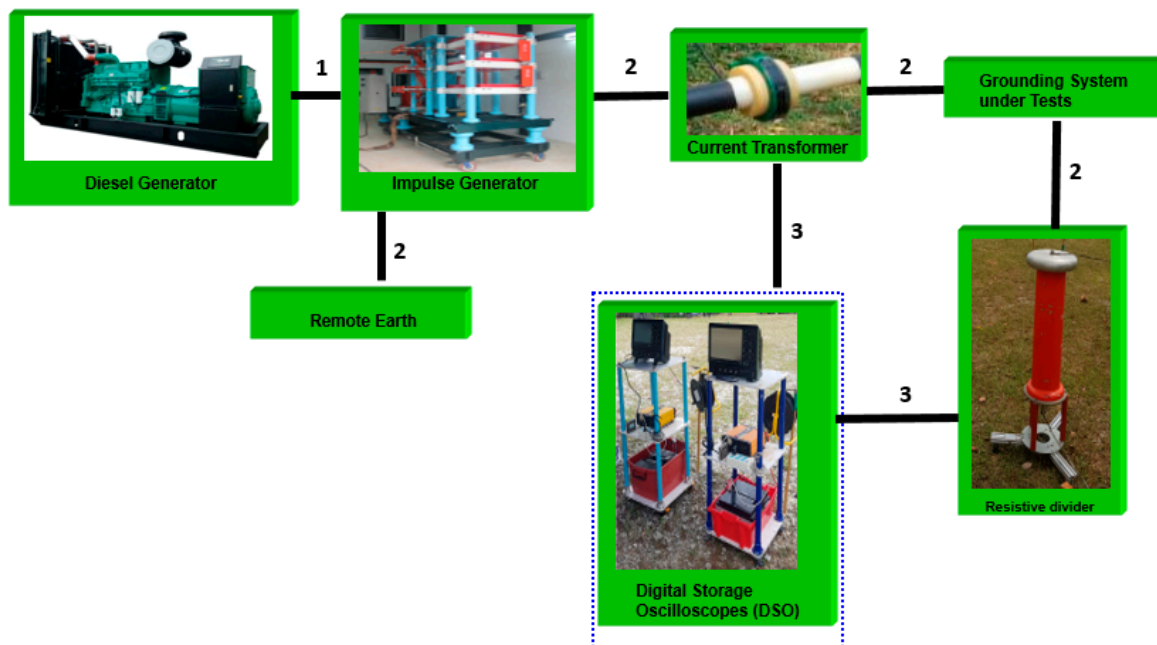
Figure 1. Impulse test set up used for testing grounding systems.

3. Experimental Results

In this work, the effectiveness of GDSR and other electrodes' arrangement in different soil resistivities, is studied. Impulse tests are conducted on all electrodes with different current magnitudes. Both voltage and current impulse shapes for all electrode configurations are found to be similar, with fast rise times and fast decay on the voltage and current traces (see Figures 2 and 3 for charging voltage at 30 kV and 150 kV, respectively) observed. However, the time to peak current, and time for current to discharge to zero, are found to be dependent on voltage magnitudes, electrode configurations and soil resistivity. For these reasons, to provide a better analysis on the performance of these electrodes under high impulse currents and various factors, the results are presented in several sub-sections; time to peak current, time to discharge to the ground, and impulse resistance for various earth electrode configurations and soil resistivity. Evidence of hysteresis can also be seen for all configurations, installed at all sites. Figure 4 shows the v–i loops for configuration 1, installed at site 2, at various levels of charging voltage. As can be seen, at lower charging voltage, 30 kV, the v–i plot shows a small

loop, while at higher charging voltage, a bigger 'loop' is formed. The authors include the dotted lines, to indicate the v–i at the front time. Similar v–i plots are obtained for other configurations, and at various sites.
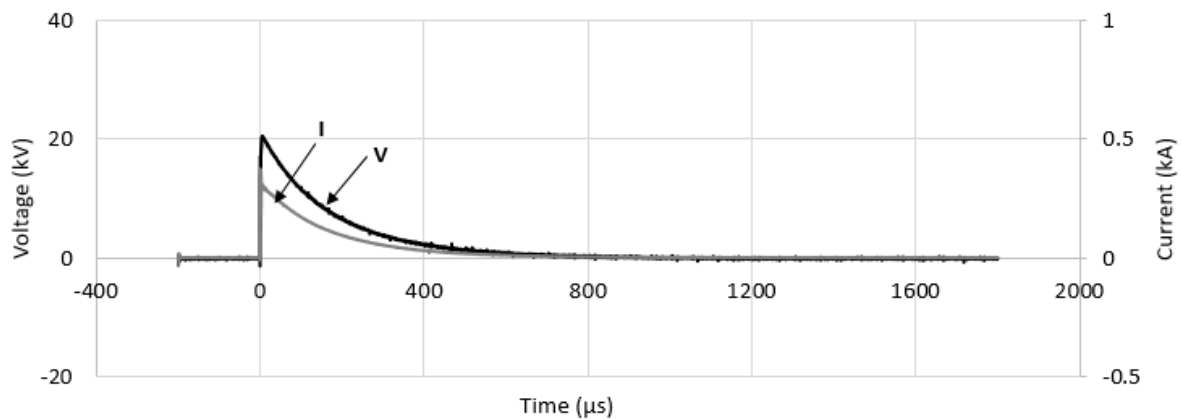
Figure 2. Voltage and current traces for configuration 1 installed at site 2, at a charging voltage of 30 kV.
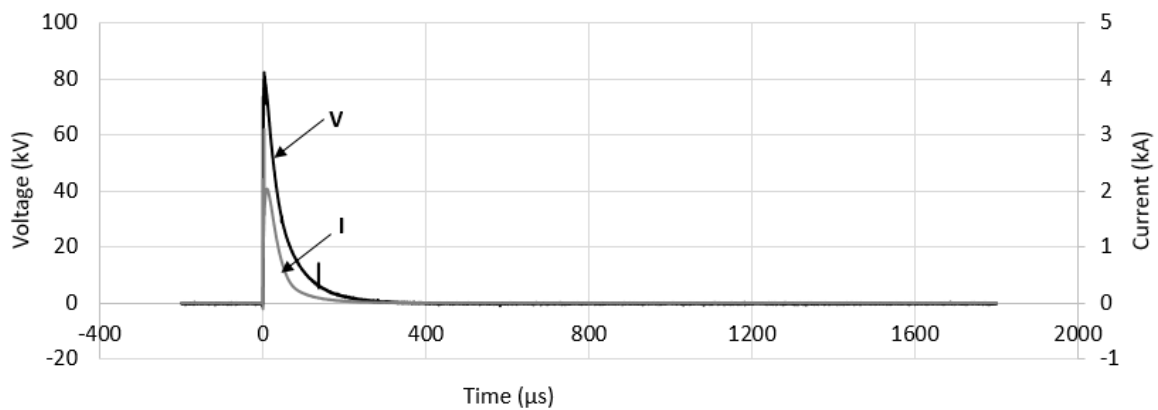
Figure 3. Voltage and current traces for configuration 2 installed at site 4, at a charging voltage of 150 kV.
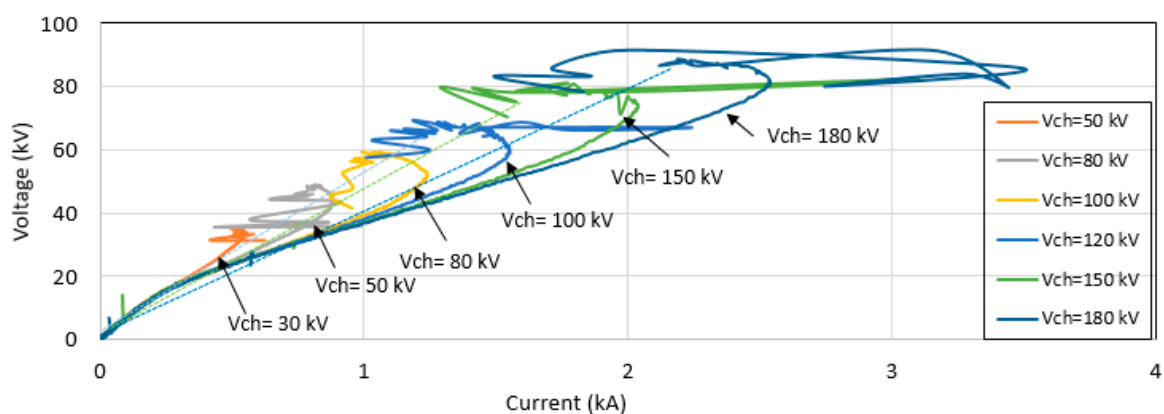
Figure 4. V–I loops for configuration 1, installed at site 2 at various levels of charging voltage.

3.1. Time to Peak Current

For all testing on tested electrodes, the charging voltage levels of the impulse generator are gradually increased. Both voltage and current impulse shapes for all electrode configurations and for all sites, are found to be similar, with fast rise times on both voltage and current traces (see Figures 2 and 3) being observed. Close examination of the current and voltage traces shows that the peak

voltage occurs at the same time as the peak current for all configurations and for all sites, indicating the resistive behavior of the earth electrodes. Figures 5–7 show the time to peak current versus the peak current for earth electrodes with different configurations and voltage magnitudes for sites 1, 2 and 3, respectively. In some studies, [22,23], the time to peak current is thought to be related to the rate of propagation of the ionization process in the soil. Thus, it would be expected that at high voltages and in high resistivity soil (high Rdc), larger ionization regions would be produced, generating a faster rate of conduction growth compared to those of low voltage and high Rdc. Their study [22] has found that the time to peak current is lower for higher conductivity soil and decreases with voltage magnitudes. Similarly, in this study, it is observed that the time to peak current is found to be at a faster rate and independent from the electrode configurations at higher current magnitudes (see Figures 5–7). When these times to current peak are plotted for each configuration for different sites, as shown in Figures 8–13, respectively, for configurations 1, 2, 3, 4, 5 and 6, it is noticed that the time to peak current for configurations 2, 3, 4, 5 and 6, at site 2, are faster than those obtained at site 1, despite these configurations at site 2 having higher Rdc than the configurations at site 1. The faster time for these configurations at site 2 could be caused by faster growth of the ionization process in high resistivity soil (site 2), which is thought to contribute to the presence of more air voids between the grains of the soil and air spaces at the interface between the soil particles and the earth electrodes in high resistivity soil. This is different than that observed in earlier mentioned publications [22], which found a faster time to peak current in low resistivity soil. Tables 5 and 6 summarise the results of different ground electrode configurations and soil resistivities, respectively, on the time to peak current.
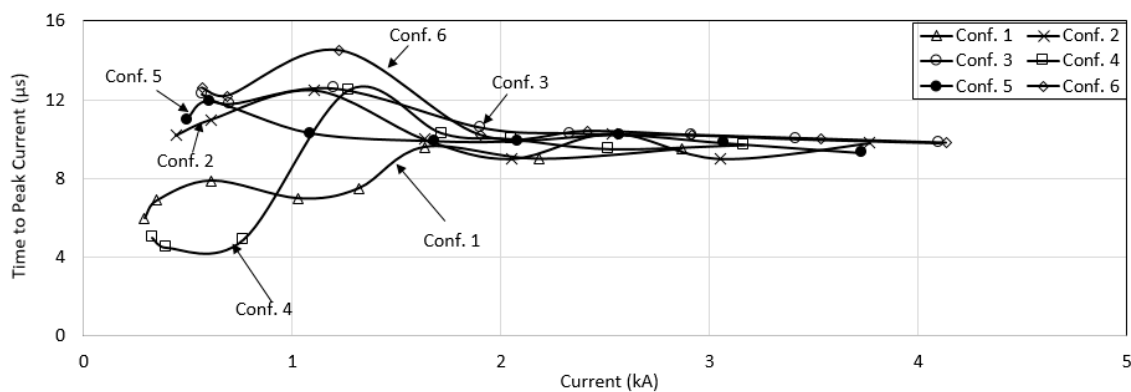
Figure 5. Time to peak current versus peak current for all configurations installed at site 1.
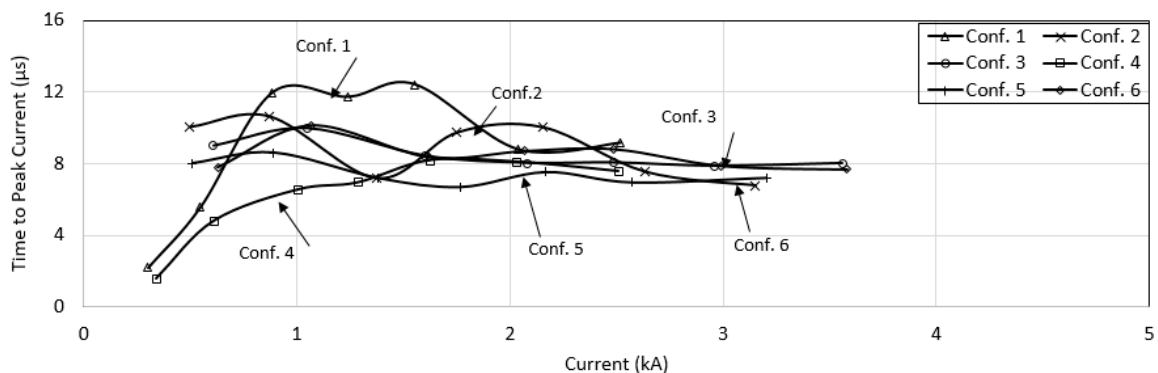
Figure 6. Time to peak current versus peak current for all configurations installed at site 2.
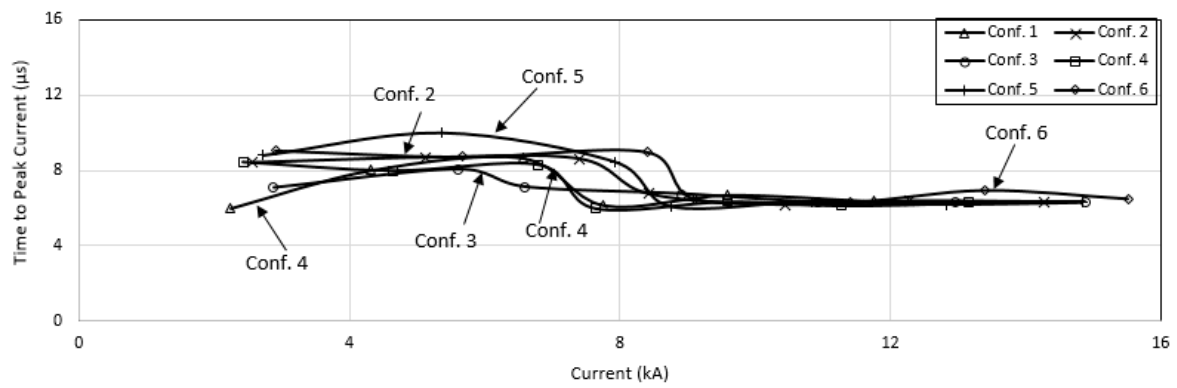
Figure 7. Time to peak current versus peak current for all configurations installed at site 3.
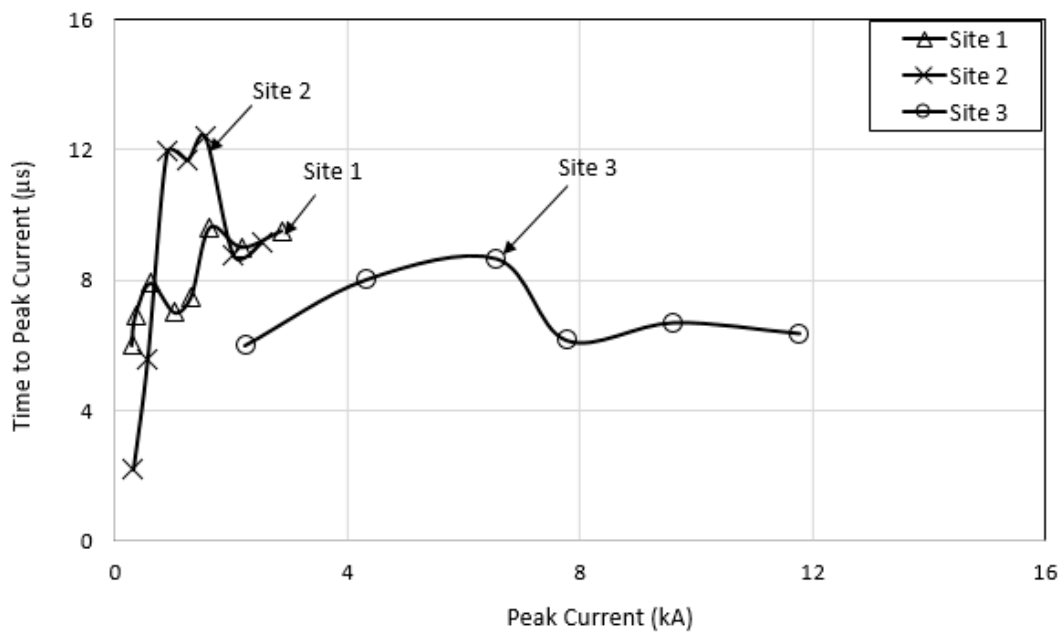
Figure 8. Time to peak current versus peak current for configuration 1 installed at all sites.
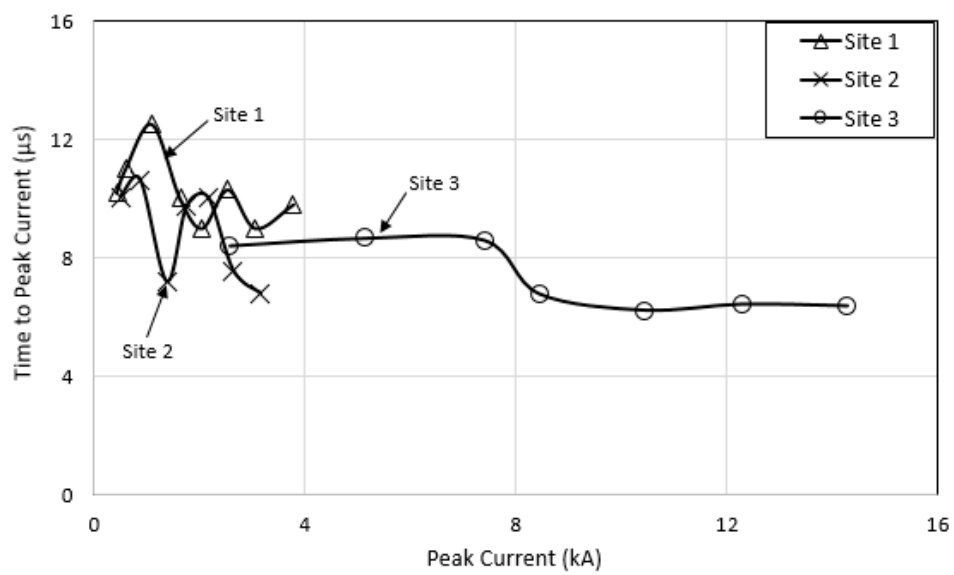
Figure 9. Time to peak current versus peak current for configuration 2 installed at all sites.
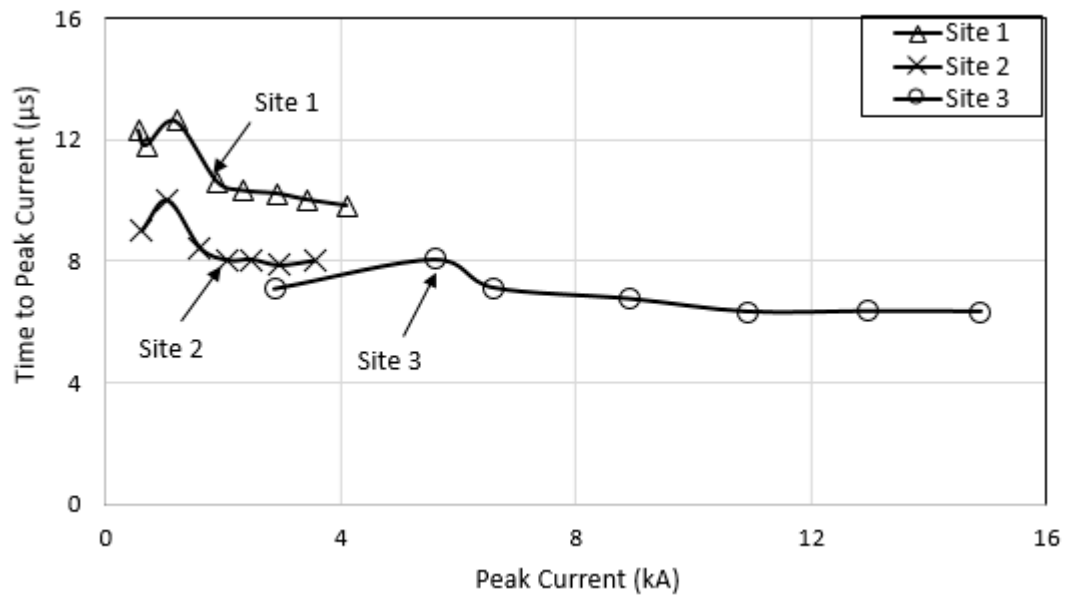
Figure 10. Time to peak current versus peak current for configuration 3 installed at all sites.
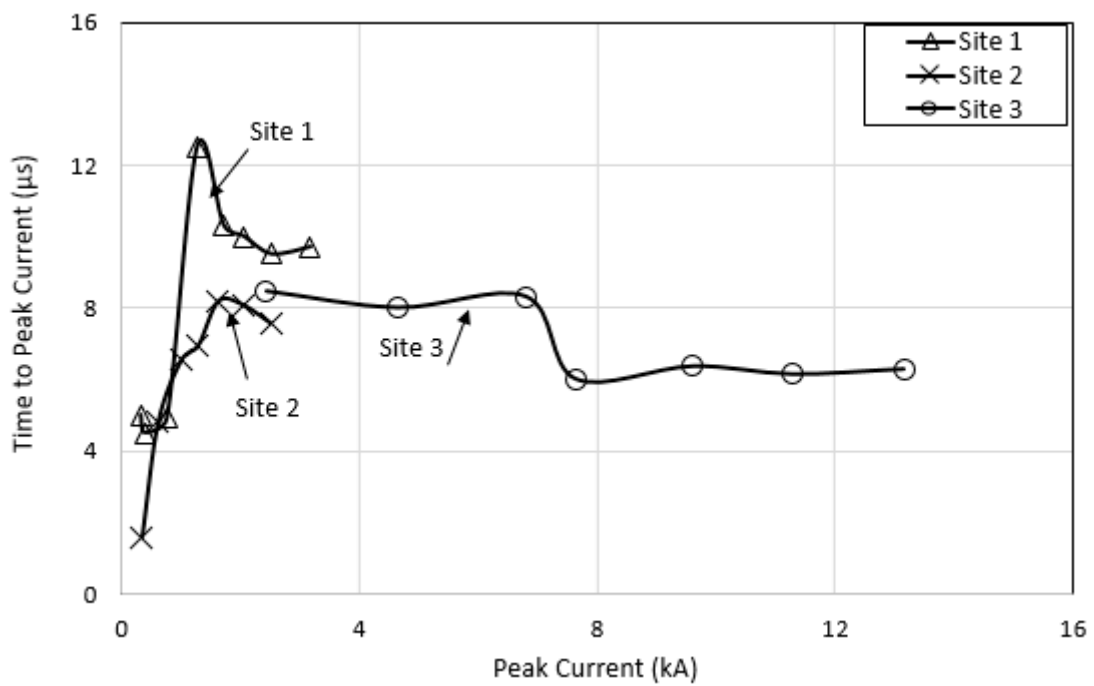
Figure 11. Time to peak current versus peak current for configuration 4 installed at all sites.
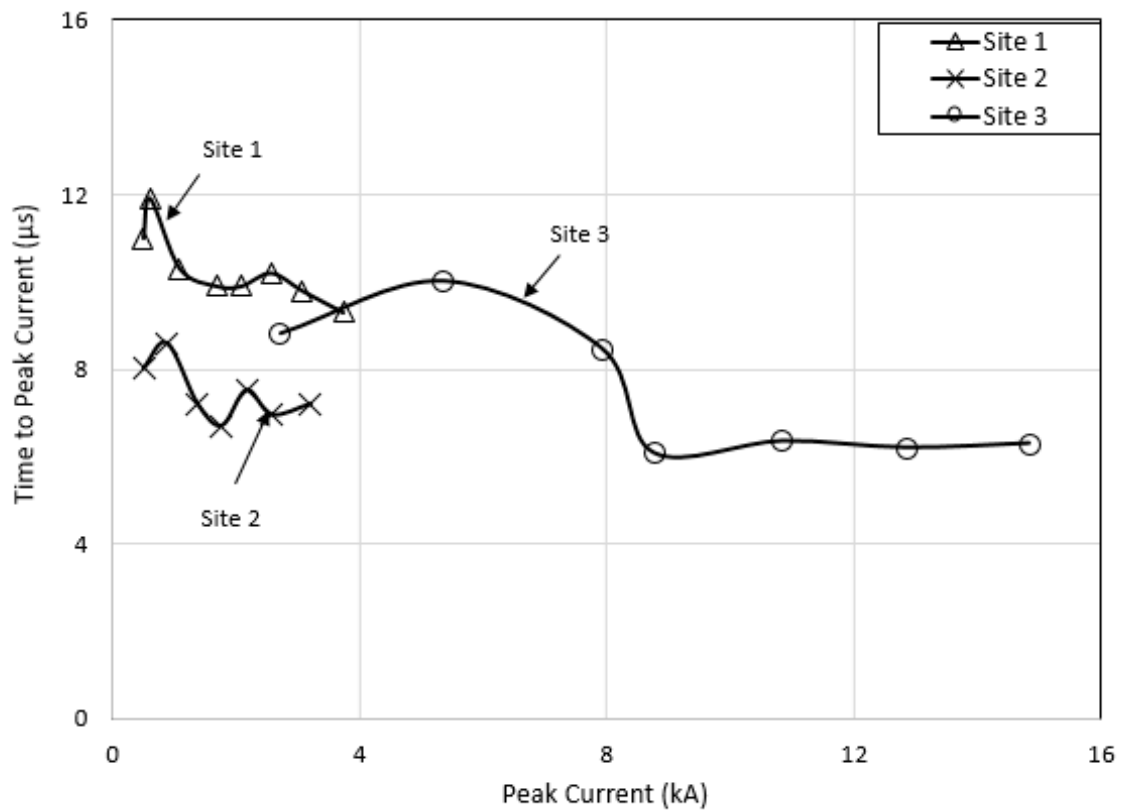
Figure 12. Time to peak current versus peak current for configuration 5 at all sites.
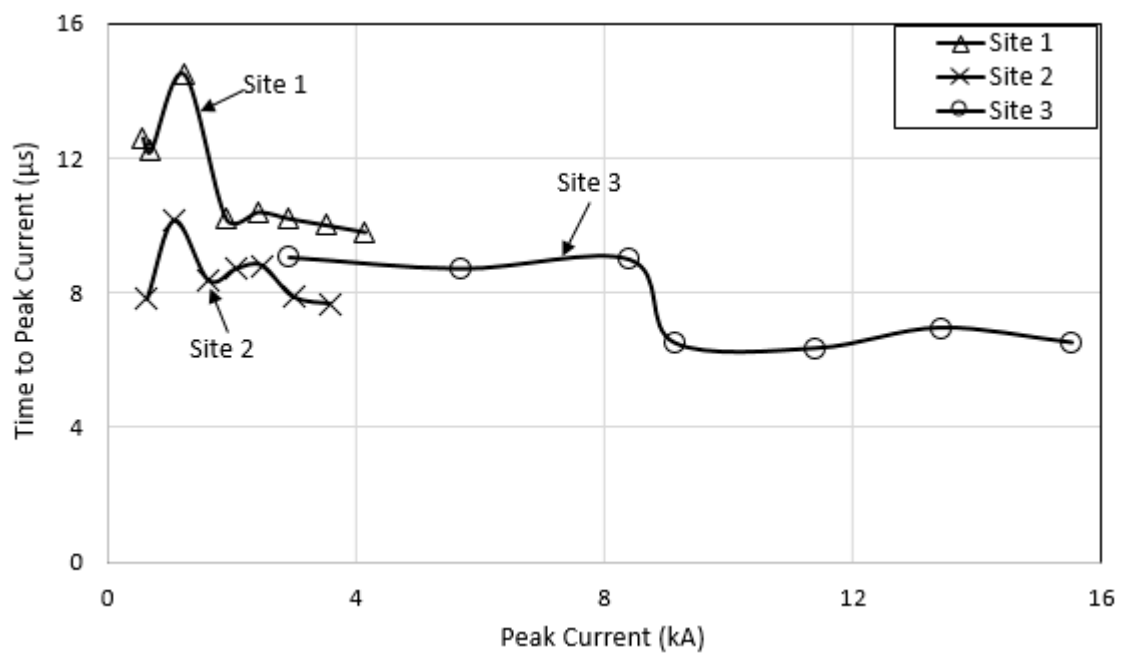
Figure 13. Time to peak current versus peak current for configuration 6 at all sites.

Table 5. Summary of the Effect of Configurations on Time to Peak Current.

Site	Time to Peak Current for Various Configurations
1	For the current magnitudes of below 2 kA, the time to peak current is dependent on the electrode configurations; conf. 6 takes the slowest time to peak current, followed by conf. 5, 4, 3, 2 and 1. For the current magnitudes of above 2 kA, the time to peak current is around 10 μs, independent of electrode configurations, constant with increasing currents
2	For the current magnitudes of below 2.5 kA, the time to peak current is dependent on the electrode configurations; conf. 1 takes the slowest time to peak current. For the current magnitudes of above 2.5 kA, the time to peak current is around 8 μs, independent of electrode configurations, constant with increasing currents.
3	For the current magnitudes of below 9 kA, the times to peak current are quite close to each other; conf. 5 takes the slowest time to peak current. For the current magnitudes of above 9 kA, the time to peak current is around 7 μs, independent of electrode configurations, constant with increasing currents.

Table 6. Summary on the Effect of Soil Resistivity on Time to Peak Current.

Configuration	Time to Peak Current at Various Sites
1	Conf. 1 installed at site 2 has the highest time to peak current. Time to peak current decreases with increasing current, for conf. 1 at all sites
2	
3	Configurations installed at site 1 have the highest time to peak current. Time to peak current decreases with increasing current, for all sites
4	
5	
6	

3.2. Time for Current to Discharge to Zero

It is observed that the time for the current trace to discharge to zero, t_o, is different for different earth electrodes and soil resistivities. As described in References [5,7,8], the time for the current to discharge to zero, t_o, indicates how effective the grounding system is in discharging high current to the ground and the resistive behavior of grounding systems, i. e. the current signal will decrease at a slower rate for relatively large values of resistance, compared to those for small resistance values. Figures 14–16 show the time for the current trace to discharge to zero, respectively, for sites 1, 2 and 3. As generally seen in the figures, the time for the current trace to discharge to zero decreases with increasing applied voltage for all sites, except for site 3, which is found to be weak dependent on applied voltage for all configurations, except for configuration 4. The decrease of time for the current trace to discharge to zero for ground electrodes installed at sites 1 and 2 is thought to be related to the resistive behavior of grounding systems. It is likely that at low voltages and for grounding systems with high Rdc, a slower rate for current signal to discharge is caused by the high value of the resistance. In this work, it is found that most earth electrodes with low Rdc have faster discharging times due to the relatively low value of the resistance in comparison to the high Rdc.
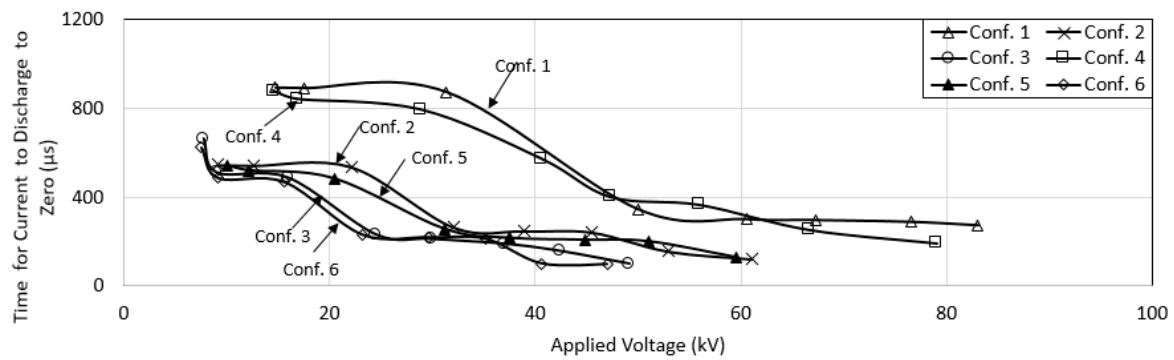
Figure 14. Time for current to discharge to zero for all configurations installed at site 1.
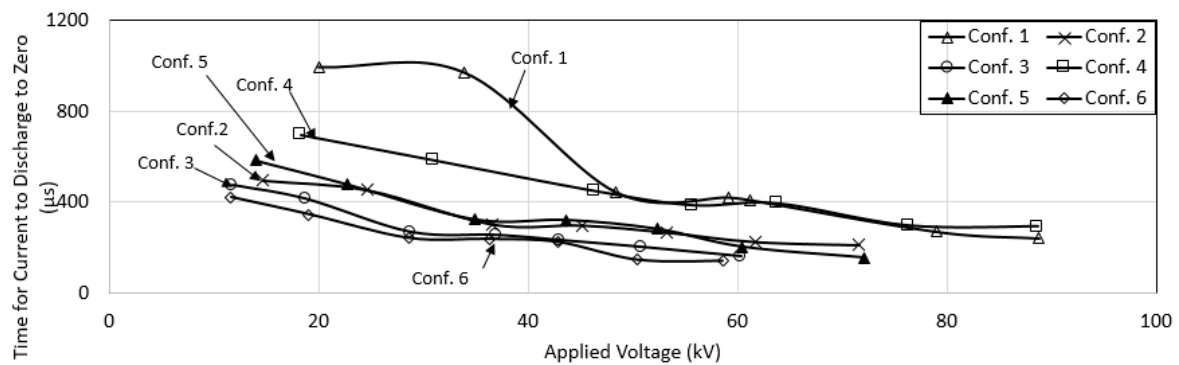
Figure 15. Time for current to discharge to zero for all configurations installed at site 2.
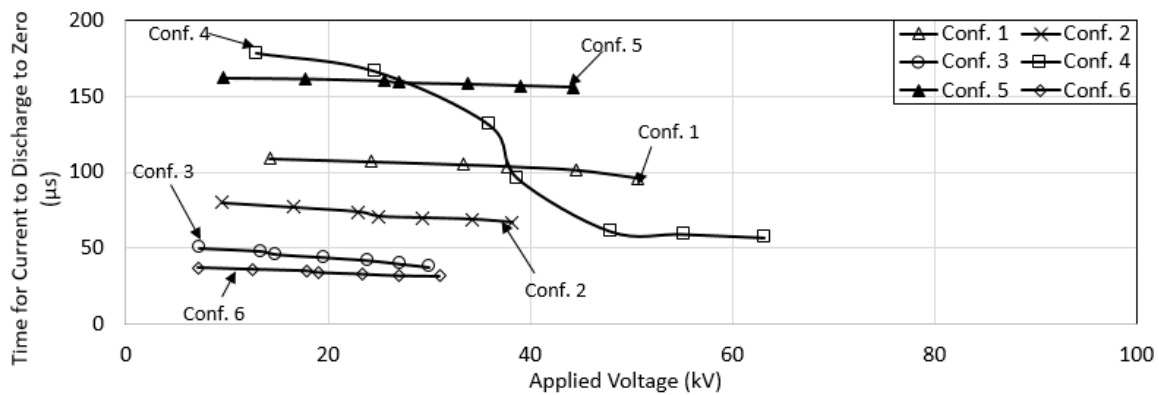
Figure 16. Time for current to discharge to zero for all configurations installed at site 3.

The times for current to discharge to zero for different sites are also compared, as shown in Figures 17–22, respectively, for configurations 1, 2, 3, 4, 5 and 6. It can be seen that the higher the Rdc and soil resistivity, the slower the time taken for currents to discharge to zero. This shows that it is important to have grounding systems with low Rdc, to provide effective discharge of the current to the ground. Tables 7 and 8 summarise the results of different ground electrode configurations and soil resistivity, respectively, on the time taken for the current to discharge to zero.
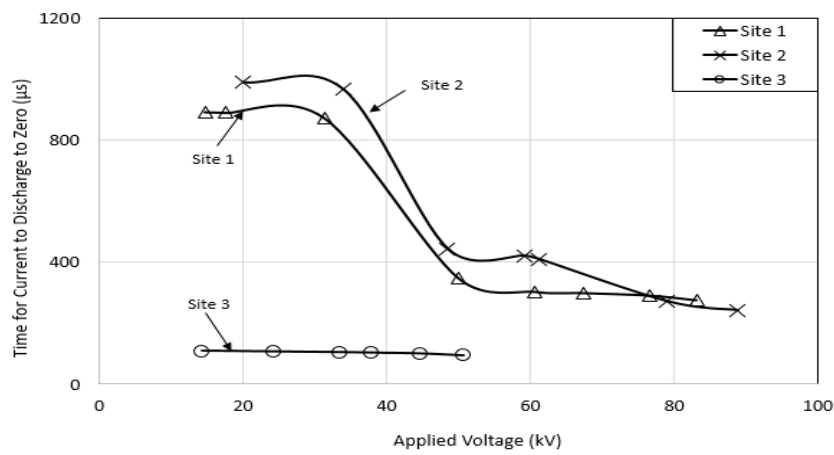
Figure 17. Time for current to discharge to zero for configuration 1 installed at all sites.
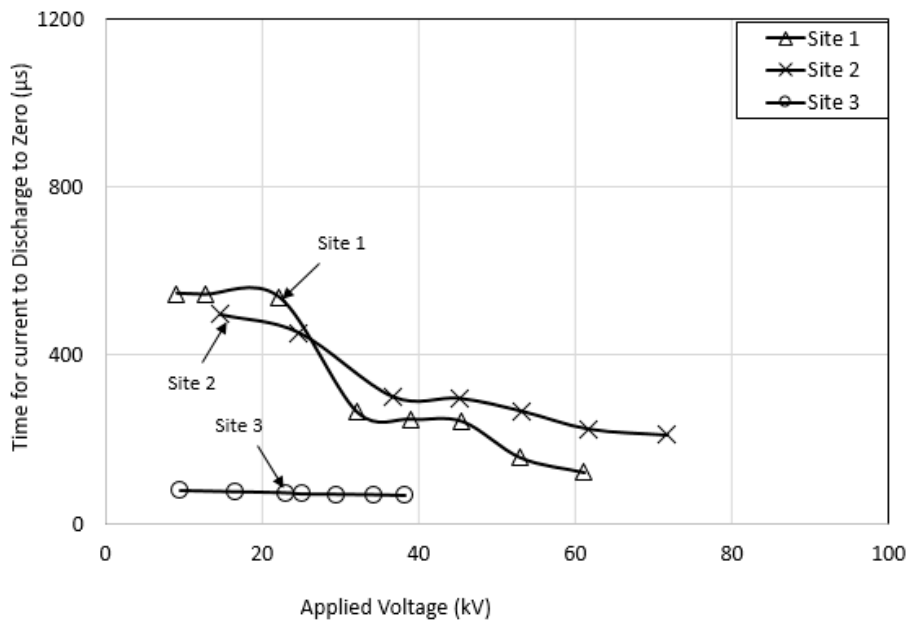
Figure 18. Time for current to discharge to zero for configuration 2 installed at all sites.
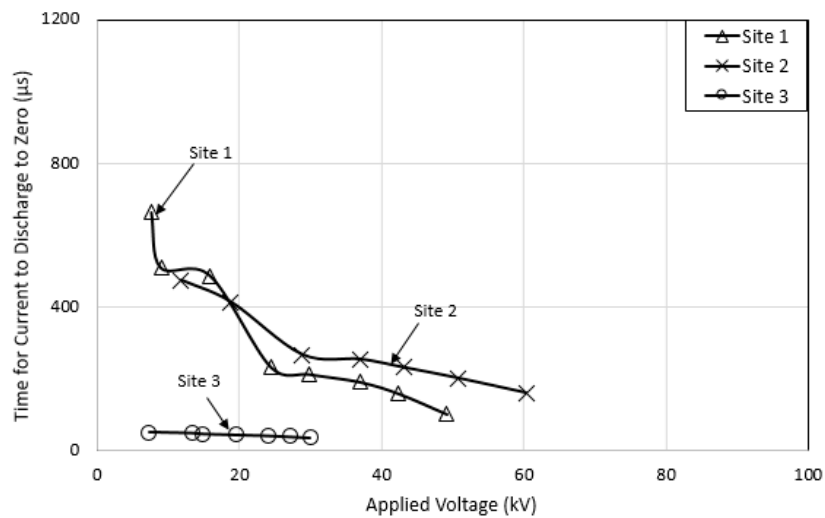
Figure 19. Time for current to discharge to zero for configuration 3 installed at all sites.
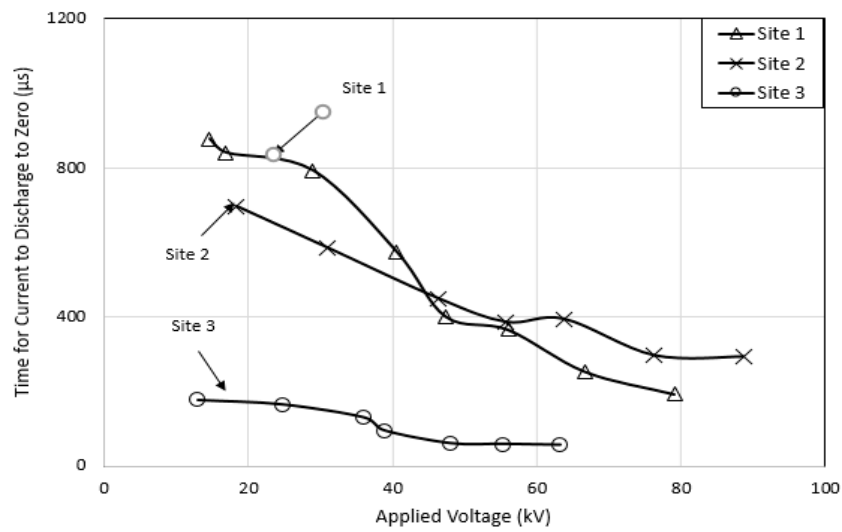
Figure 20. Time for current to discharge to zero for configuration 4 installed at all sites.
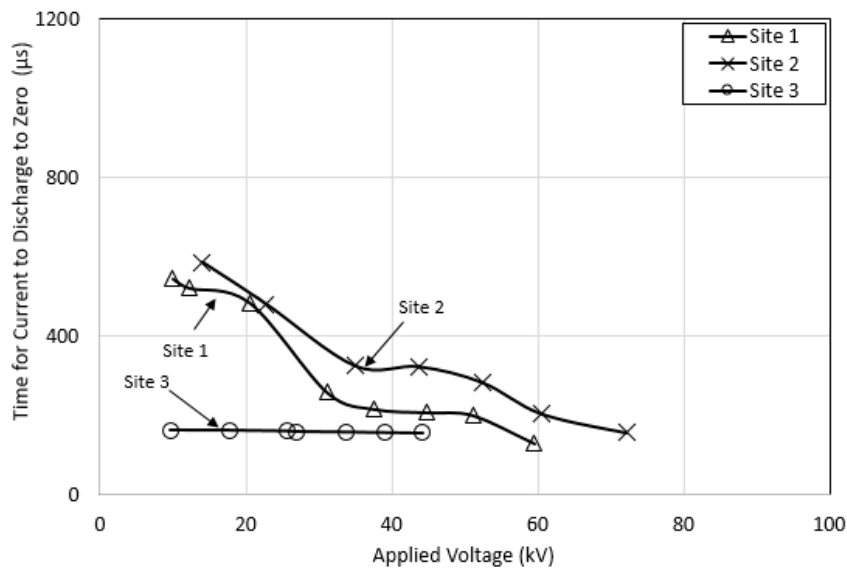
Figure 21. Time for current to discharge to zero for configuration 5 installed at all sites.
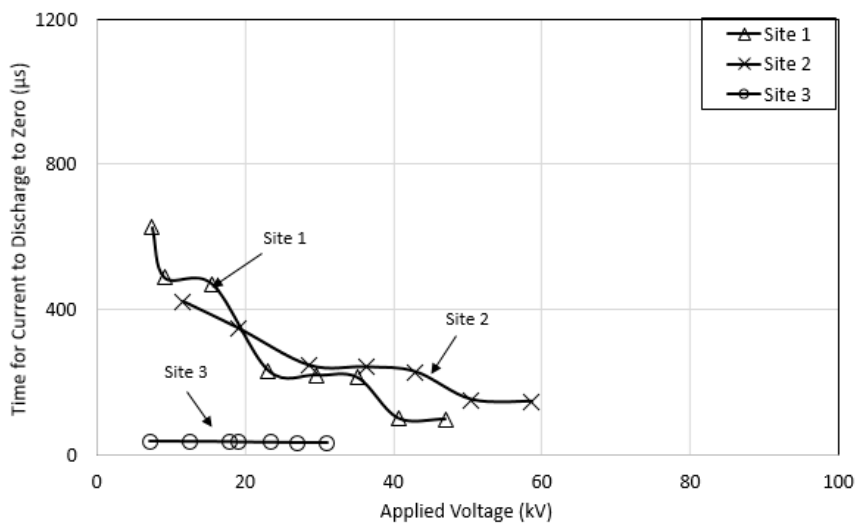
Figure 22. Time for current to discharge to zero for configuration 6 installed at all sites.

Table 7. Summary on the Effect of Configurations on Time for Current to Discharge to Zero.

Site	Time for Current to Discharge to Zero for Various Configurations
1	The time for the current to discharge to zero decreases with increasing applied voltage for all configurations.
2	Configuration 1 takes the slowest time for the current to discharge to the ground, followed by configuration 4, 2, 5, 3 and 6. This trend shows that the time for the current to discharge to the ground is highly dependent on Rdc values, where the higher the Rdc value, the longer the time taken for the current to discharge to zero.
3	Only configuration 4 has a significant reduction of time for the current to discharge to zero with increasing applied voltage, while the time for the current to discharge to zero for other configurations is nearly constant with increasing applied voltage, hardly dependent on Rdc values.

Table 8. Summary of the Effect of Soil Resistivity on Time for Current to Discharge to Zero.

Configuration	Time for Current to Discharge to Zero at Various Sites
1	
2	
3	All configurations installed at sites 1 and 2 have the time for the current to discharge to zero decrease with increasing applied voltage, while configurations installed at low soil
4	resistivity (site 3) are almost constant with increasing applied voltage (except for configuration 4).
5	
6	

3.3. Impulse Impedance, $Z_{impulse}$

In this study, $Z_{impulse}$ values are estimated and expressed as the ratio of the peak voltage to the peak current, as suggested in previously published work [5,7,8]. It is observed that the impulse resistance decreases with increasing currents for configuration 1 for all sites, whereas $Z_{impulse}$ is found to be independent of the current magnitudes for other configurations (see Figures 23–25, respectively, for sites 1, 2 and 3). This could be caused by high Rdc values of configuration 1, in comparison to other Rdc values, as presented in Table 2. The findings are similar to those obtained in many studies [7,8], [10,11] and [22], showing that the degree of non-linearity of soil conduction is dependent on Rdc ground resistance values, in which the lower the Rdc is, the lower the rate of reduction of $Z_{impulse}$ with increasing current is.
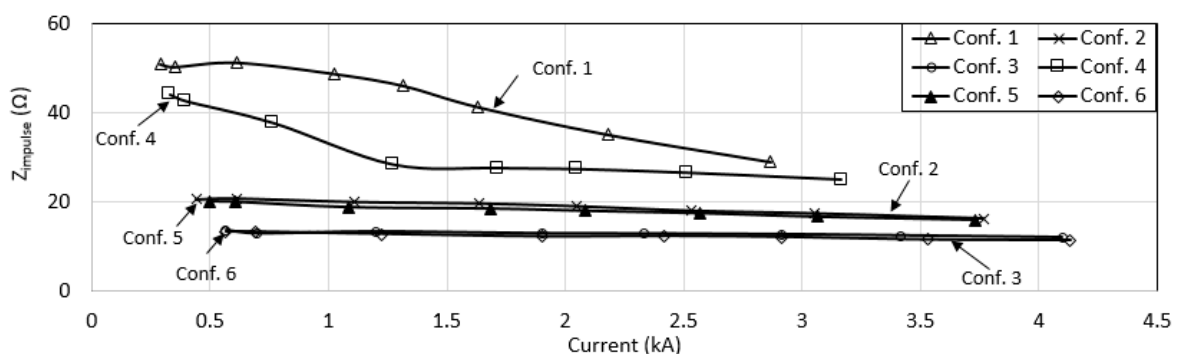
Figure 23. $Z_{impulse}$ for all configurations installed at site 1.
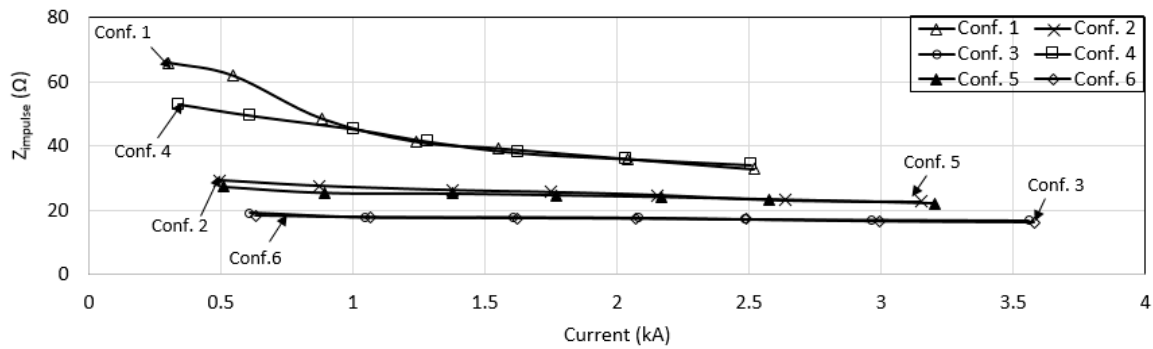
Figure 24. $Z_{impulse}$ for all configurations installed at site 2.
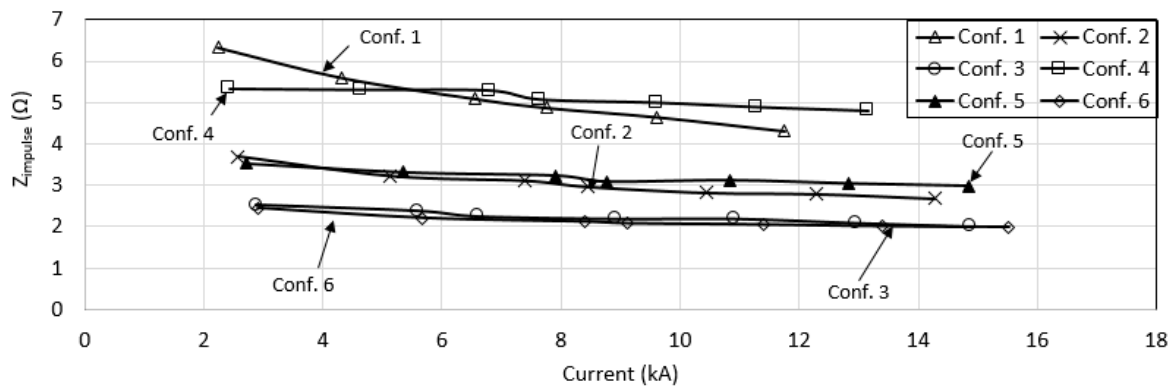
Figure 25. $Z_{impulse}$ for all configurations installed at site 3.

It was also found that $Z_{impulse}$ is relatively low in low resistivity soil. It is also observed that the earth electrodes in high resistivity soil (site 4) have a significant reduction in $Z_{impulse}$ with increasing current magnitudes (for all configurations) and the reduction in $Z_{impulse}$ becomes less current-dependent for earth electrodes in low resistivity soil (site 3). This is similar to the results observed in References [5–20], which suggested that the decrease in $Z_{impulse}$ with current magnitudes is due to an ionisation process in the soil. In high resistivity soil, more field enhancement could have taken place due to more air voids, hence more non-linearity in $Z_{impulse}$, in comparison to low resistivity soil.

When $Z_{impulse}$ values for each configuration for different sites are compared, it shows that $Z_{impulse}$ values are low for configurations 2, 3, 4, 5 and 6 in site 3, followed by site 1, due to their low resistivity and relatively low Rdc. Figures 26–31, respectively, show configurations 1, 2, 3, 4, 5 and 5 installed at all three sites. However, for configuration 1, little difference in $Z_{impulse}$ values for both sites 1 and 2 is observed. Tables 9 and 10 summarise the results of different ground electrode configurations and soil resistivity, respectively, on the $Z_{impulse}$.

Table 9. Summary of the Effect of Configurations on Impulse Impedance, $Z_{impulse}$.

Site	Time for Current to Discharge to Zero for Various Configurations
1	
2	The higher the Rdc, the higher is the $Z_{impulse}$ for all sites.
	The non-linearity, or reduction of $Z_{impulse}$ with increasing current is clearly seen for configurations 1
3	and 4 (high Rdc). While, $Z_{impulse}$ is almost constant with increasing current for other configurations.
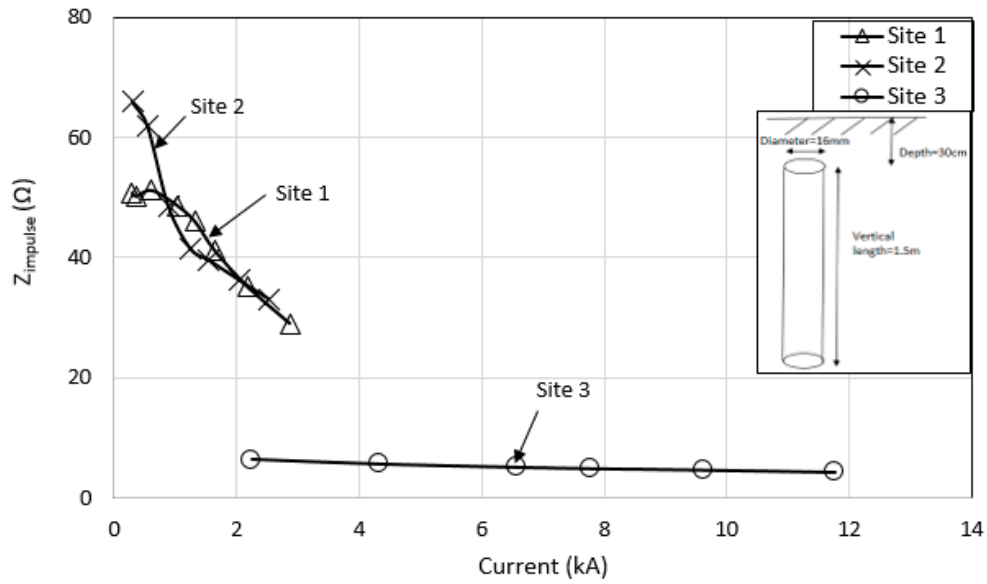
Figure 26. $Z_{impulse}$ for configuration 1 installed at all sites.
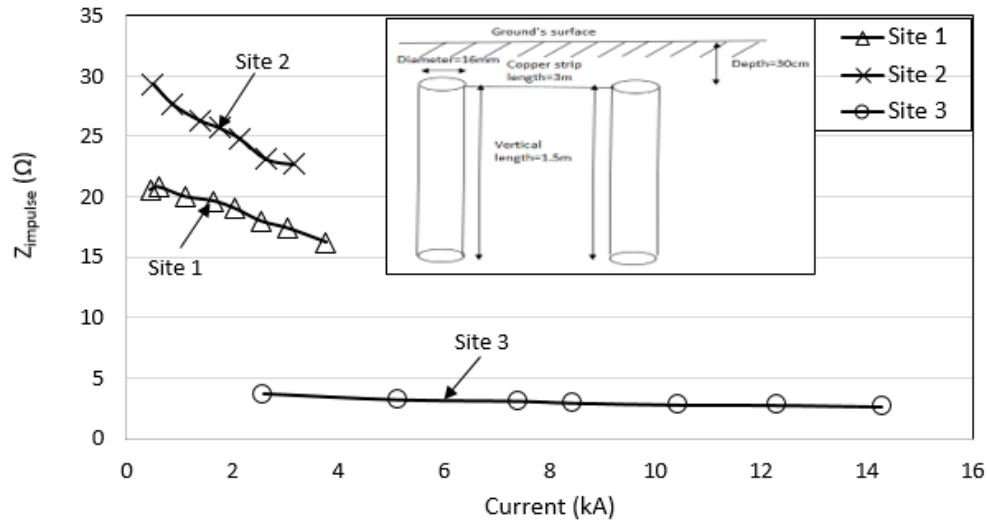
Figure 27. $Z_{impulse}$ for configuration 2 installed at all sites.
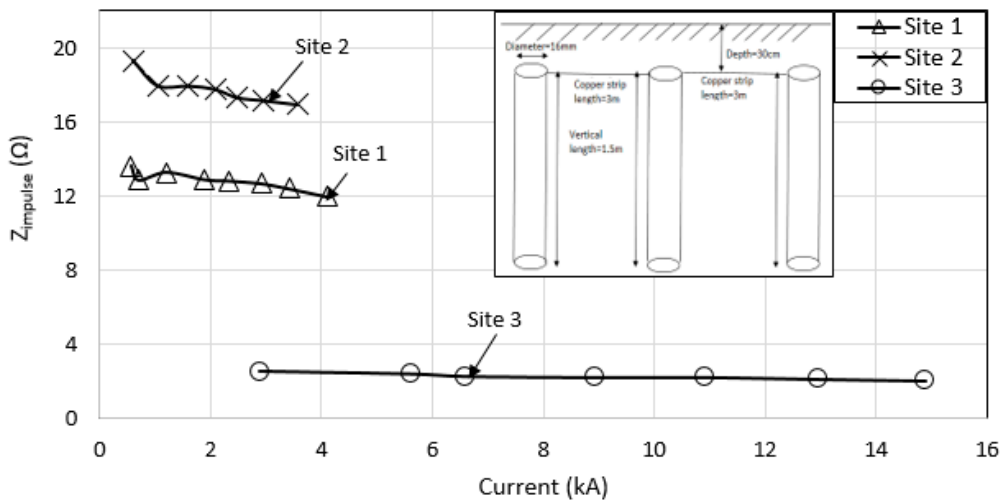
Figure 28. $Z_{impulse}$ for configuration 3 installed at all sites.
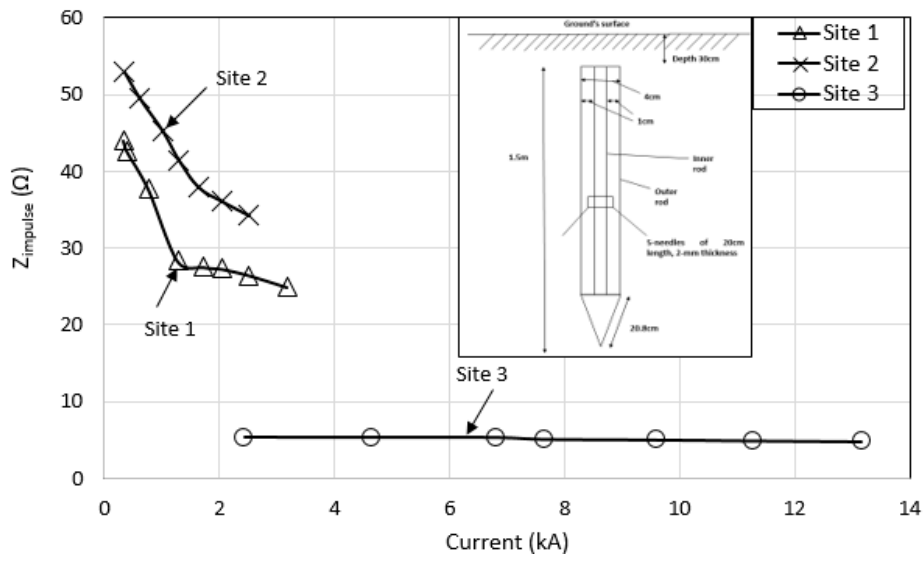
Figure 29. $Z_{impulse}$ for configuration 4 installed at all sites.
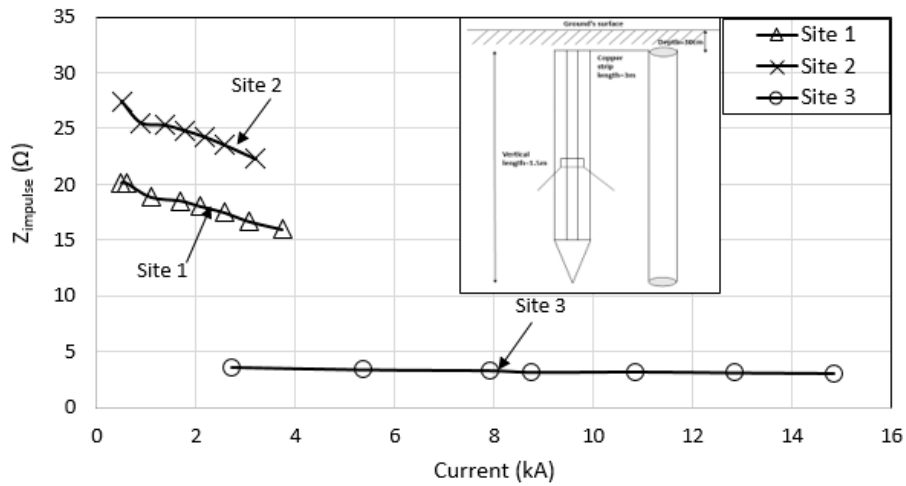
Figure 30. $Z_{impulse}$ for configuration 5 installed at all sites.
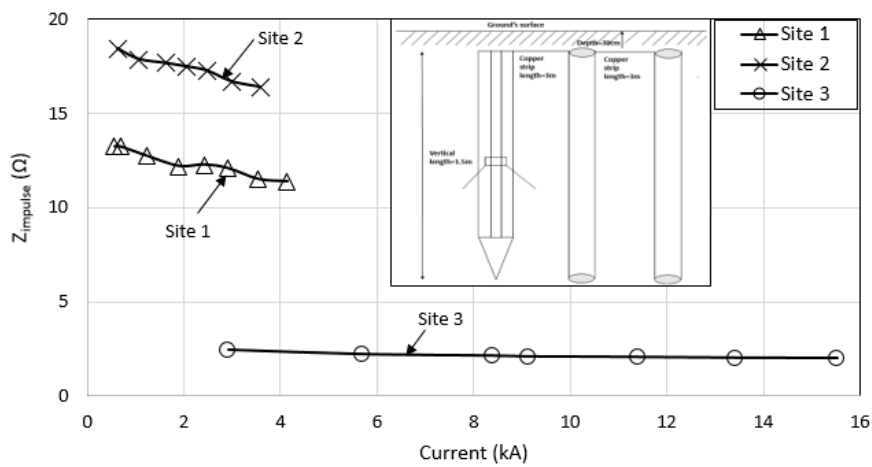
Figure 31. $Z_{impulse}$ for configuration 6 installed at all sites.

Table 10. Summary of the Effect of Soil Resistivity on Impulse Impedance, $Z_{impulse}$.

Configuration	$Z_{impulse}$ at Various Sites
1	Close $Z_{impulse}$ values for configuration 1 installed at sites 1 and 2. A significant reduction in $Z_{impulse}$ values with increasing current for configuration 1 installed at sites 1 and 2, while $Z_{impulse}$ are almost constant, independent of current magnitudes for configuration 1 installed at site 3, due to low soil resistivity.
2	$Z_{impulse}$ values for configurations 2–6 installed at site 2 are always higher than those installed at site 1.
3	
4	A significant reduction in $Z_{impulse}$ values for configurations installed at sites 1 and 2, while $Z_{impulse}$ values are almost constant, independent of current magnitudes for configurations installed at site 3, due to low soil resistivity.
5	
6	

4. Simulation Work

4.1. Simulation Set up

In this paper, Finite Element Method (FEM) COMSOL Multiphysics software is used to obtain the electric field profile of each configuration installed at three sites. For each configuration, three layers of medium are considered, i.e., air, upper soil layer and bottom soil layer are modelled in FEM, where the conductivity of soil is an inverse of the soil resistivity values, presented in Table 2 for the three sites, with the electrical conductivity of the air at 1.8×10^{-14}, as suggested in [24]. FEM is first used to compute for Rdc values for each configuration, installed at all sites. Earth electrodes are carefully drawn and modelled, close to the materials, configurations and installation depth of tested ground electrodes, as presented in Section 2 of this paper, i.e., the rod electrodes are 1.3 m inside the ground and 0.2 m in the air (see Figure 32). For this simulation, 1 A current was injected into the grounding system, and –1 A current was injected to the return electrode. A relative permittivity value of 1 was used for air, while 9 was used for soil. The relative permittivity, ε_r was assumed as 9 throughout the simulation, based on the published work by Srisakot et al. [25], who found that the ε_r was in a range of 5 to 12 for sand mixed with 1% to 10% percent of water content. It was also listed in [26] that the ε_r ranged between 4 and 6, and 10 and 30, respectively, for dry and wet sand. Due to the condition of the original soil, which had some mixture of water content, the ε_r of 9 was used, which is the value between the ε_r of dry and wet sand. This ε_r of 9 is also close to the value used in Reference [18], which was 10. However, it was noticed that no difference in electric field profile was seen when ε_r was changed to 40. This is because, the main parameters that change the electric field profile are the soil resistivity, or electrical conductivity of the soil that surrounds the ground electrode, which are pre-dominant factors, in comparison to ε_r. These electrical conductivity values are inverse to the soil resistivity, shown in Table 2. For the FEM simulation of electrodes under high impulse conditions, current signals obtained from experimental work are injected into the ground electrode, while the electric field values are measured at the bottom of rod electrodes.

Simulation of Rdc values was also computed, using the MALZ module of the CDEGS [19]. The two-layers soil resistivity profile computed using the RESAP module of the CDEGS [19] was used in this simulation, where the results are presented in Table 2. In CDEGS [19], the grounding system is defined as installed 0.3 m below the ground's surface. A return conductor, having a length of 200 mm and a diameter of 8 mm, with its embodiment made of stainless steel, is placed 10 m from configurations 1 and 4, 20 m away from configurations 2 and 5, and 30 m away from configurations 3 and 6. These distances of return conductor are based on the suggested distance in IEEE Standard 81 [4], in which the return conductor needs to be placed at least five times the largest/diagonal length of the grounding grid. The same placement of the return conductor for the current, which is defined as the current probe, is also used during the measurement of Rdc for all configurations, at all sites. For conventional rod electrodes, 40% copper-clad steel, and the GDSR made of stainless steel, are defined in the CDEGS [19] simulation.
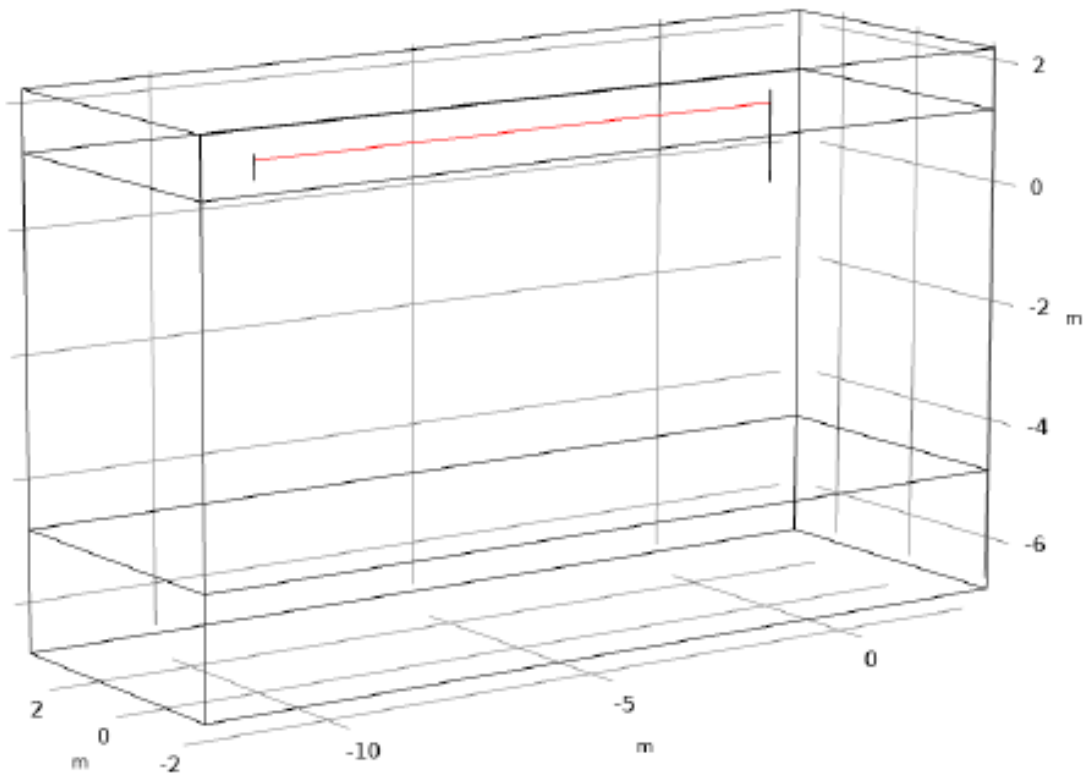
Figure 32. Example of a Finite Element Method (FEM) model used for configuration 1.

4.2. Computed Results

Figure 33 shows the typical Rdc graph obtained by FEM computation for configuration 1, at site 1. Similar graphs are seen for other configurations, and at various sites. Table 11 shows the experimental and simulated test results. Close computed results are obtained for FEM and CDEGS [19]. However, as can be seen in Table 11, measured results are found to be different than the computed results, which can be due to the factors mentioned in IEEE Std 81 [4], such as the existence of nearby metallic structures and ground wires, the presence of reactance in the test circuit which may come from the grounding electrodes and the cables used during the testing, and reactance from the test circuit and large size of the grounding grid. In order to minimize the discrepancies between the calculated values, where the calculated values rely heavily on the accuracy of the earth resistivity measurement, as is suggested in IEEE Std 81 [4], the soil resistivity measurements are carried out on the same day as Rdc measurements. Differences between measured and calculated results can also be seen in previous work [8,26]. In this paper, measured results of Rdc are used as a reference throughout the paper, similar to those presented in [8,26], when CDEGS [19] were utilized and where measured results were used as a reference and comparison to the Z_{impulse} obtained under high impulse conditions.
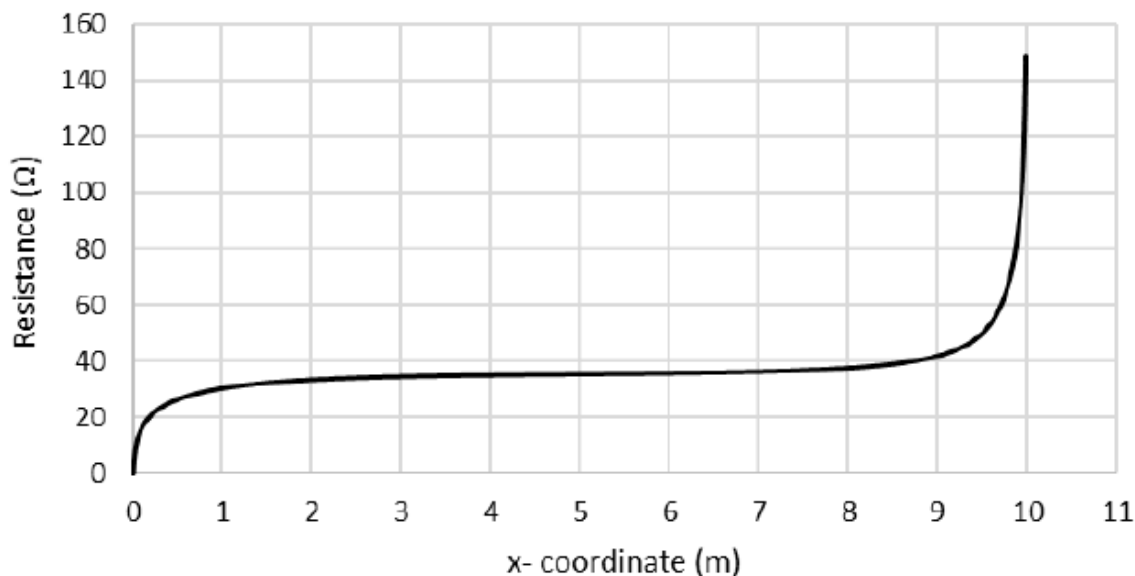
Figure 33. Typical Rdc versus observation point distance for configuration 1 at site 1.

Table 11. Measured and Computed Rdc Values for Tested Electrodes of Various Configurations Installed at Various Sites.

Conf.	Earth Electrode	Rdc Values (Ω)								
		Site 1			Site 2			Site 3		
		Meas.	Comp.		Meas.	Comp.		Meas.	Comp.	
			FEM	CDEGS		FEM	CDEGS		FEM	CDEGS
1	A vertical single rod electrode	67.02	35.4	34.9	104.4	100.1	97.1	75.52	1.84	1.7
2	2 parallel vertical rod electrodes	25.02	13.3	15.2	44.8	36.5	40.3	27.56	0.68	0.65
3	3 parallel vertical rod electrodes	16.6	18.3	10.2	28.5	23.14	26.1	17.81	0.43	0.42
4	GDSR	53.0	25.4	28.3	67.2	71.1	78.3	18.5	1.31	1.37
5	GDSR in parallel with vertical one rod electrode	23.4	11.78	14.2	37.6	32.9	39.4	14.6	0.61	0.61
6	GDSR with spike rods in parallel with two vertical rods	16.21	7.69	10.3	26.6	21.5	26.8	11.33	0.4	0.38

In the simulated results, electric field values at rod electrodes are labelled as sections A, B and C, whereas copper strips are presented as sections D and E. Figures 34–39 show the distribution of electric field, respectively for configurations 1, 2, 3, 4, 5 and 6, installed at site 1. Similar electric field profiles are seen for the same configurations installed at sites 2 and 3. Figures 40–45 show the highest values of electric field at the rod electrode, installed at all sites, respectively for configurations 1, 2, 3, 4, 5 and 6. As can be seen from Figures 39–44, for the same configurations, configurations installed at site 2 (with the highest soil resistivity) have the highest electric field. Large differences between electric field values for site 2 and the others are observed, particularly at high current magnitudes, with more than 70% difference in range at high current magnitudes between site 2 and the others. It is the same case for the configurations with the copper strips (i.e., configurations 2, 3, 5 and 6, as shown, respectively, in Figures 46–49), where the copper strips are indicated as sections D and E, and the highest electric field values are observed for configurations installed at site 2, followed by sites 1 and 3. As is expected, the electric field is high in a high level of soil resistivity. Despite lower current magnitudes in high resistivity (site 2), configurations installed at site 2 show the highest electric field, indicating that soil resistivity is a predominant contributing factor to electric field values. This is also similar to the

$Z_{impulse}$ results presented in Section 3.1, in which all $Z_{impulse}$ values of most ground electrodes are the highest for configurations installed at site 2. When electric field values at rod electrodes are plotted for all configurations installed at all sites, as shown in Figures 50–52 for sites 1, 2 and 3, respectively, it can be seen that configuration 4 has the highest electric field, followed by configurations 1, 5, 2, 6 and 3 at all sites. Therefore, for a similar configuration, configurations with GDSR have higher electric field values than the conventional electrodes. Significant differences are observed as the current magnitudes are increased, while electric field values of all configurations for site 3 (with the lowest soil resistivity) are almost constant, independent of current magnitudes. This is similar to the $Z_{impulse}$ values of configurations at site 3, which are found to be independent of current magnitudes.
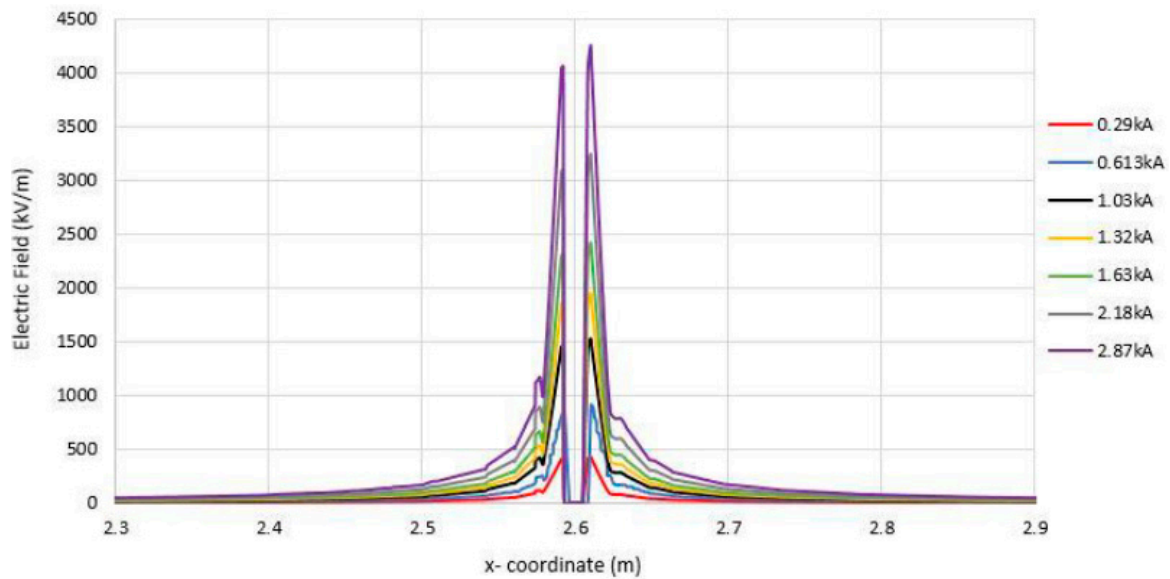
Figure 34. Typical electric field distribution for configuration 1.
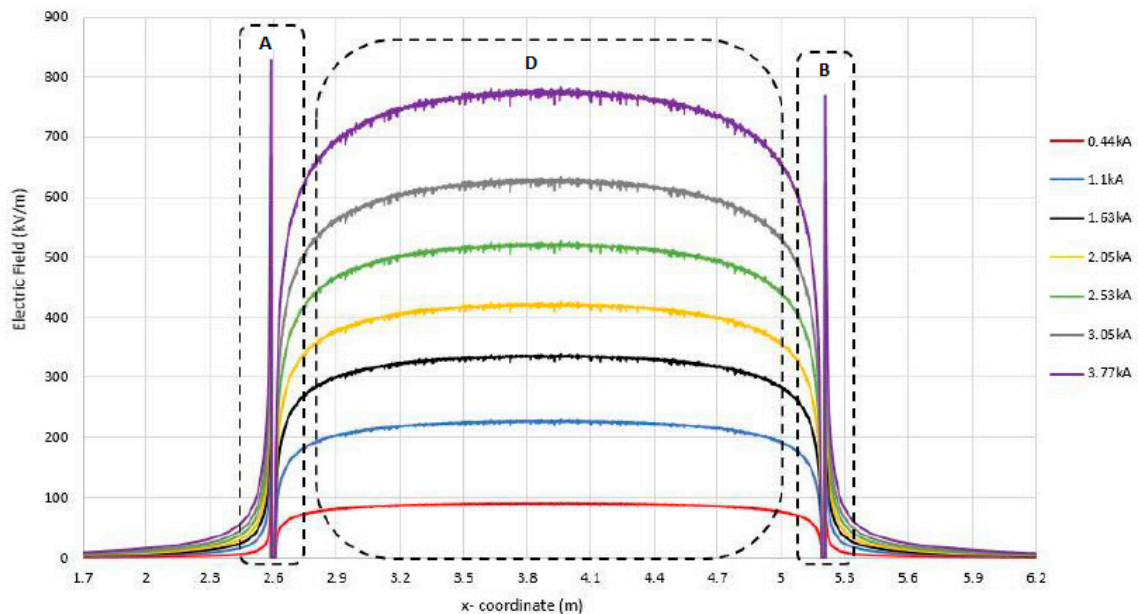
Figure 35. Typical electric field distribution for configuration 2.
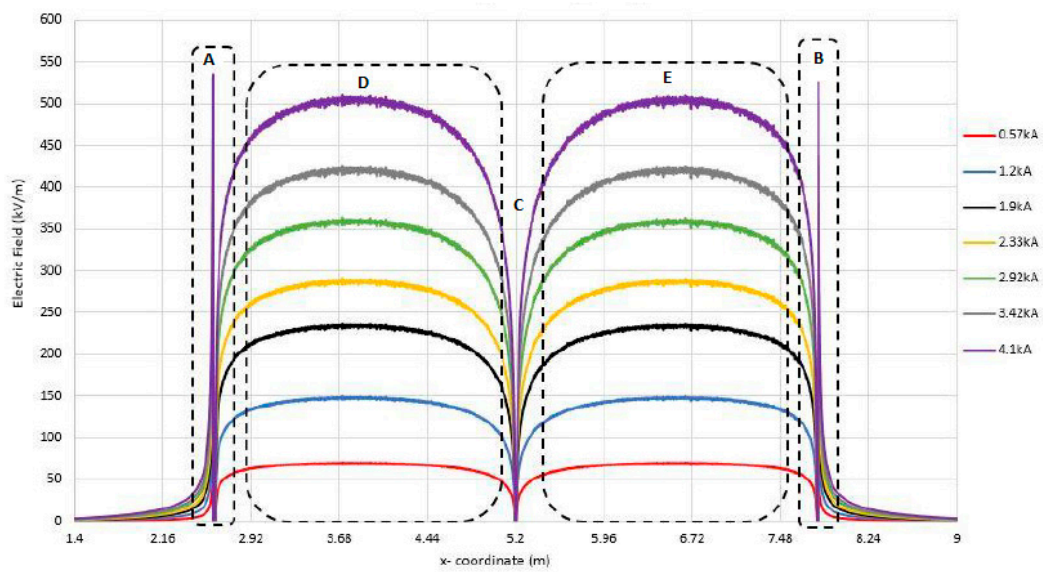
Figure 36. Typical electric field distribution for configuration 3.
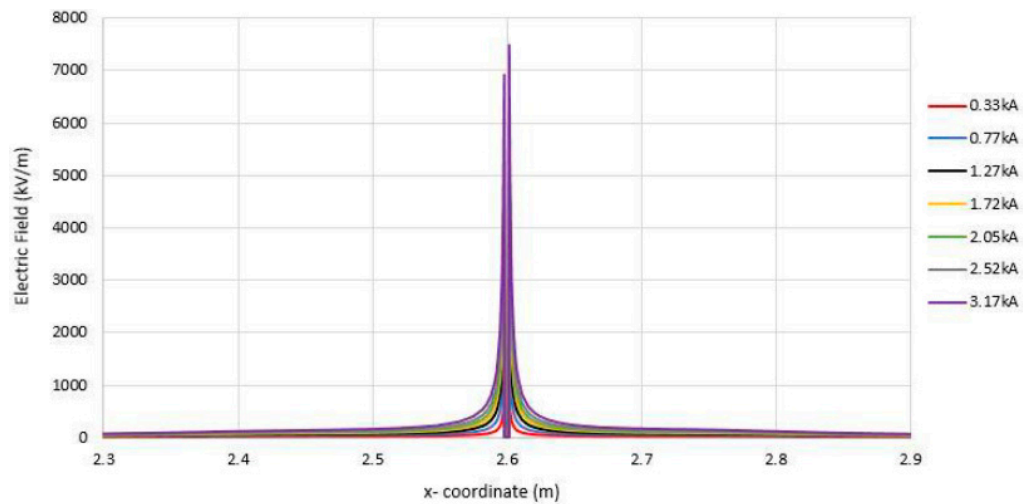
Figure 37. Typical electric field distribution for configuration 4.
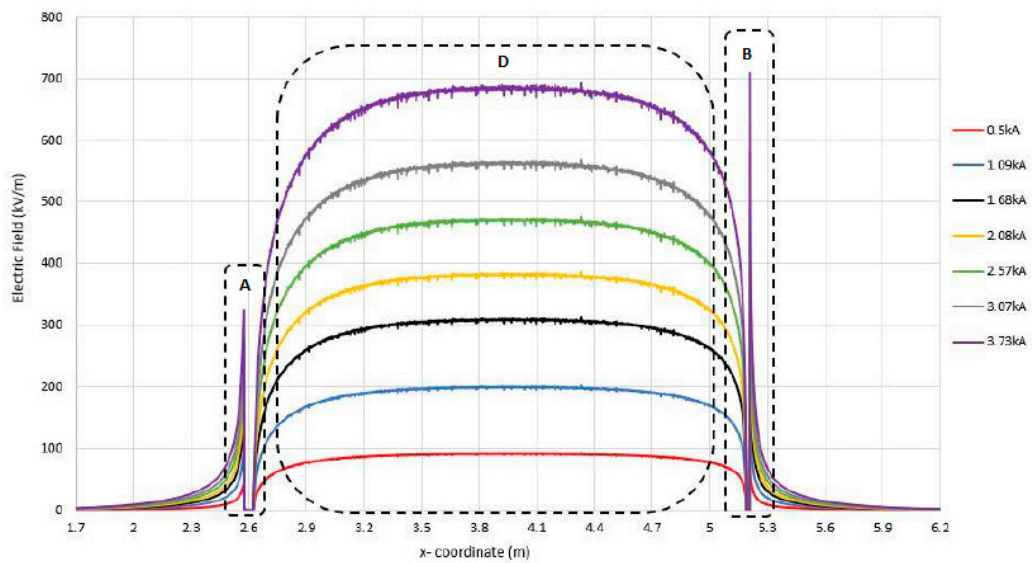
Figure 38. Typical electric field distribution for configuration 5.
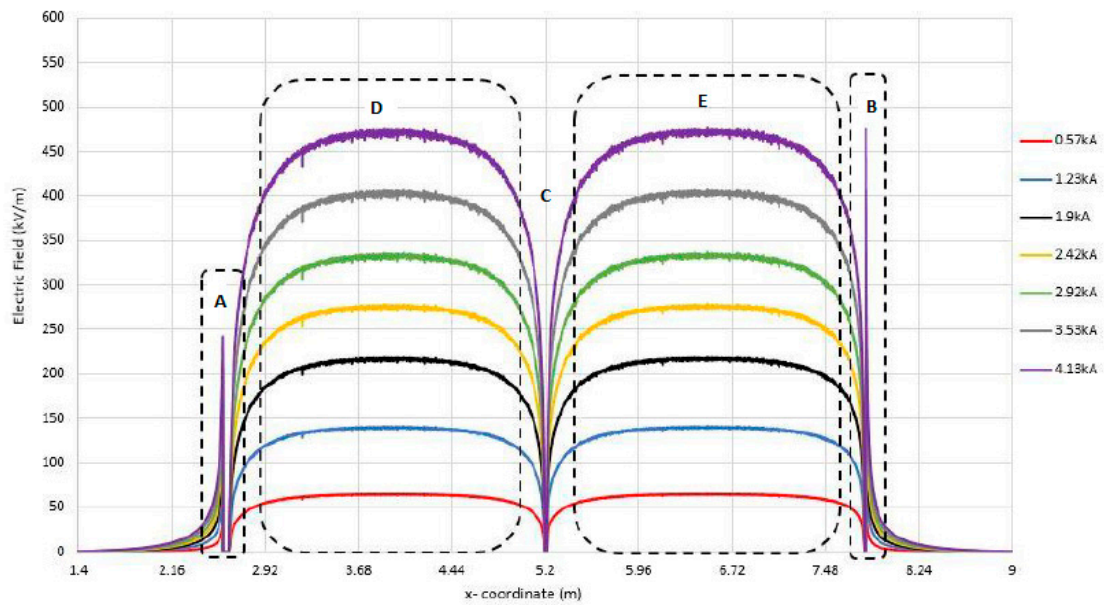
Figure 39. Typical electric field distribution for configuration 6.
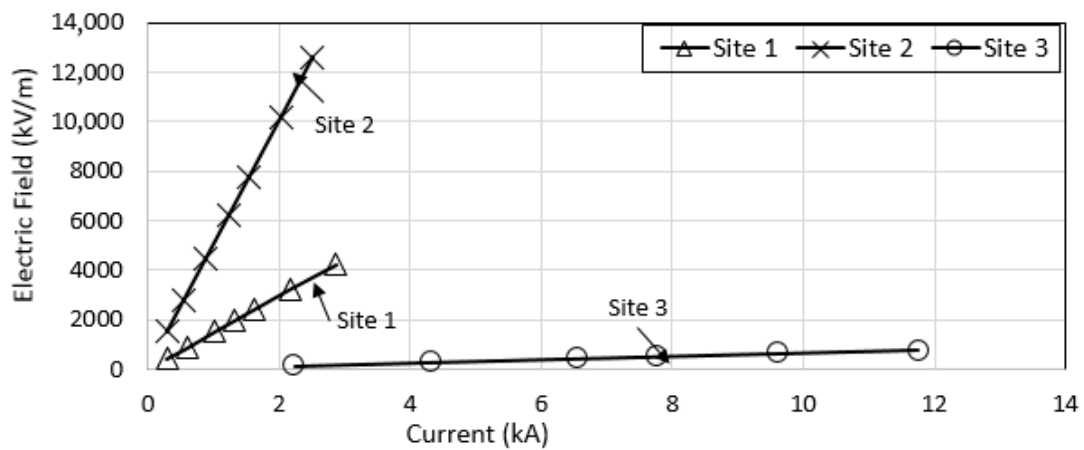
Figure 40. Highest electric field values at rod electrode, versus applied current for configuration 1, installed at various sites.
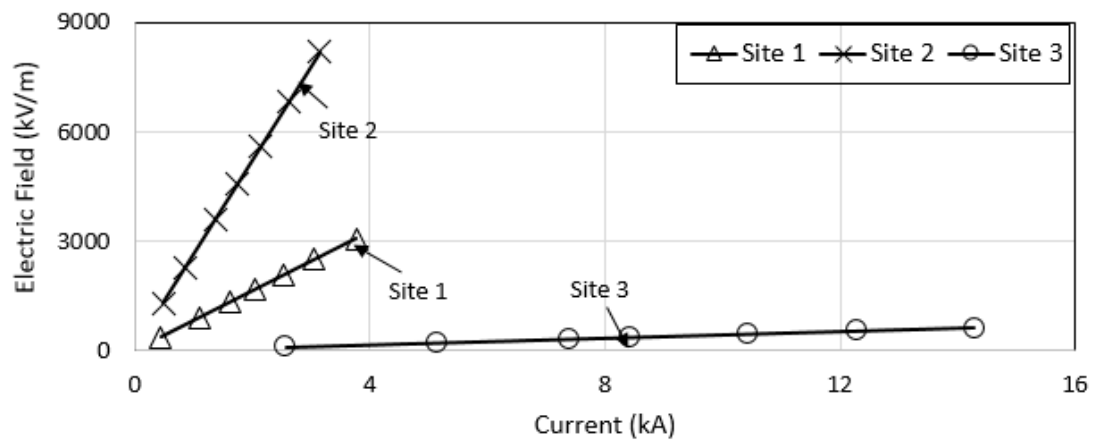
Figure 41. Highest electric field values at rod electrodes versus applied current for configuration 2, installed at various sites.
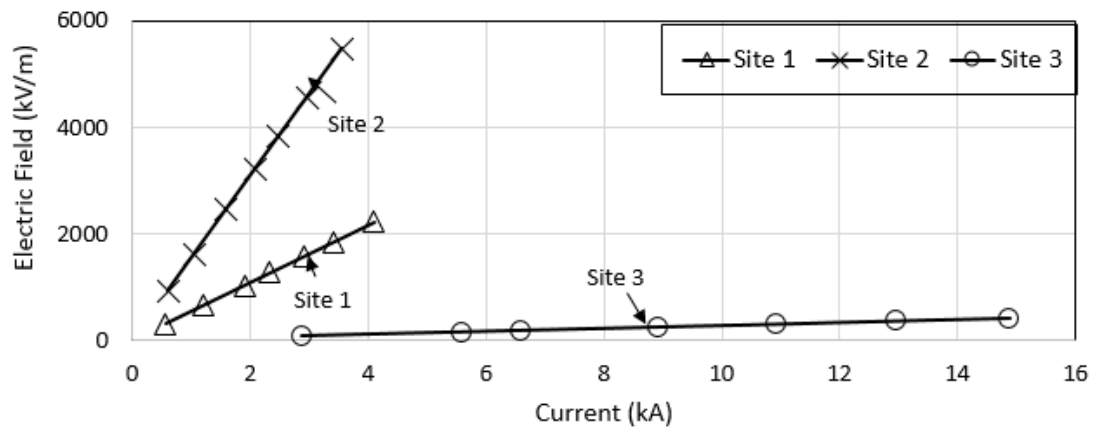
Figure 42. Highest electric field values at rod electrodes versus applied current for configuration 3, installed at various sites.
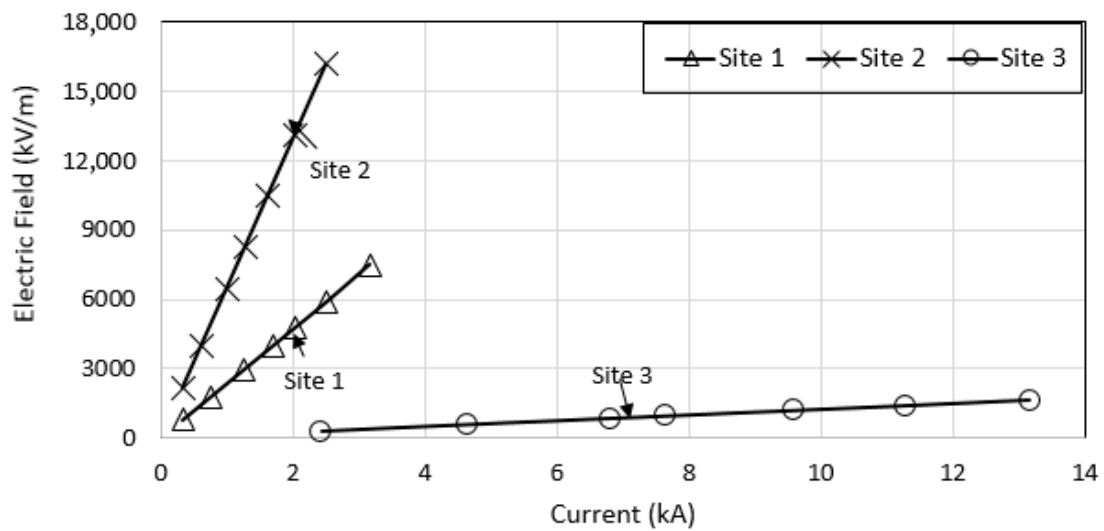
Figure 43. Highest electric field values at rod electrodes versus applied current for configuration 4, installed at various sites.
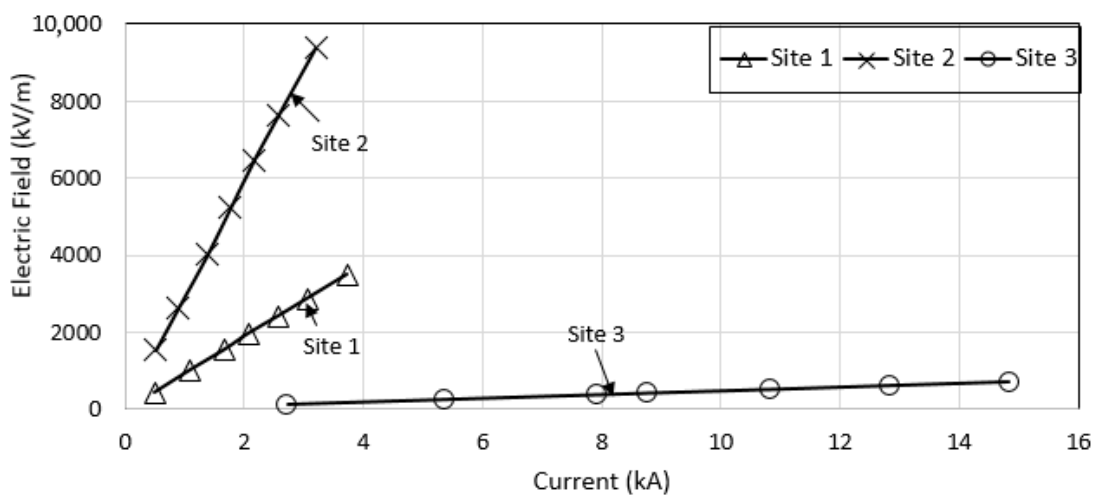
Figure 44. Highest electric field values at rod electrodes versus applied current for configuration 5, installed at various sites.
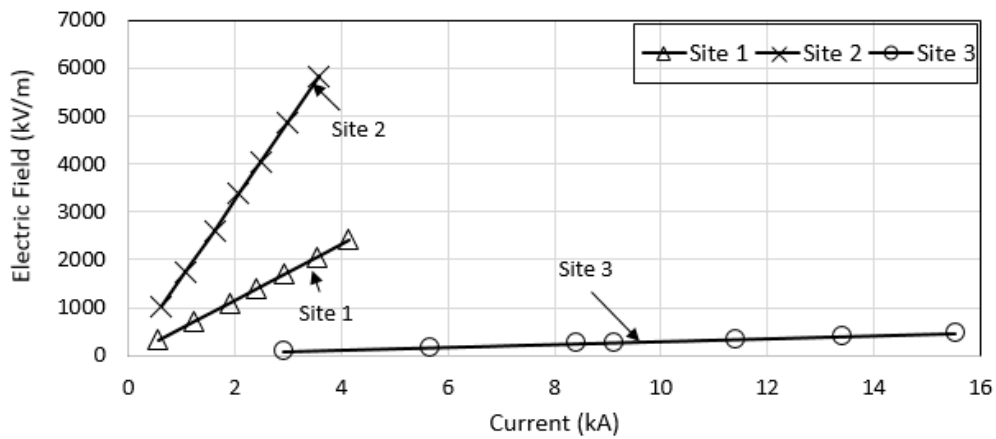
Figure 45. Highest electric field values at rod electrodes versus applied current for configuration 6, installed at various sites.
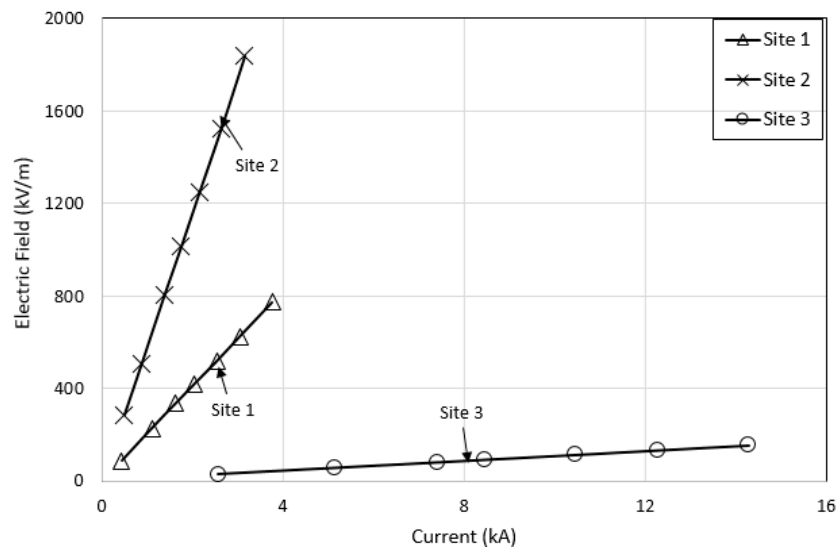
Figure 46. Highest electric field values at strip conductor versus applied current, for configuration 2, installed at various sites.
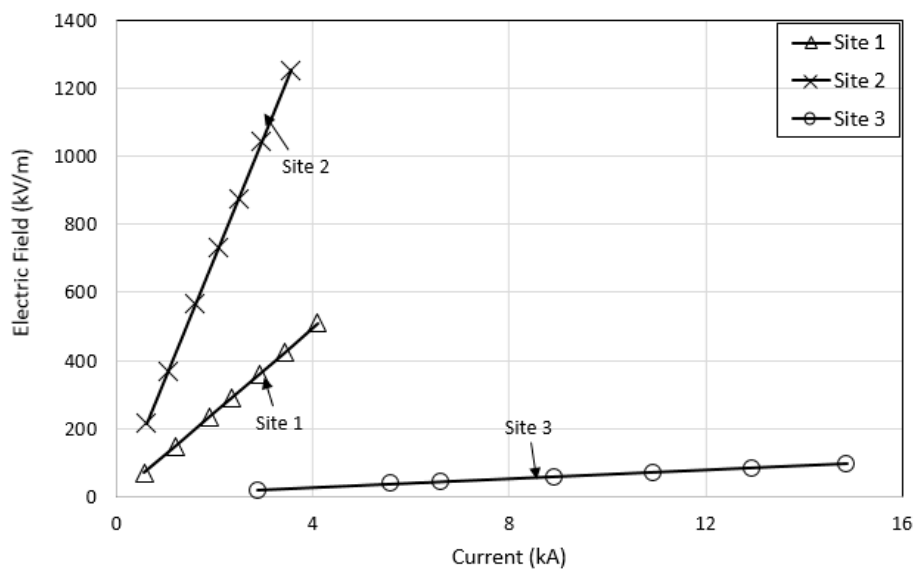
Figure 47. Highest electric field values at strip conductor versus applied current, for configuration 3, installed at various sites.
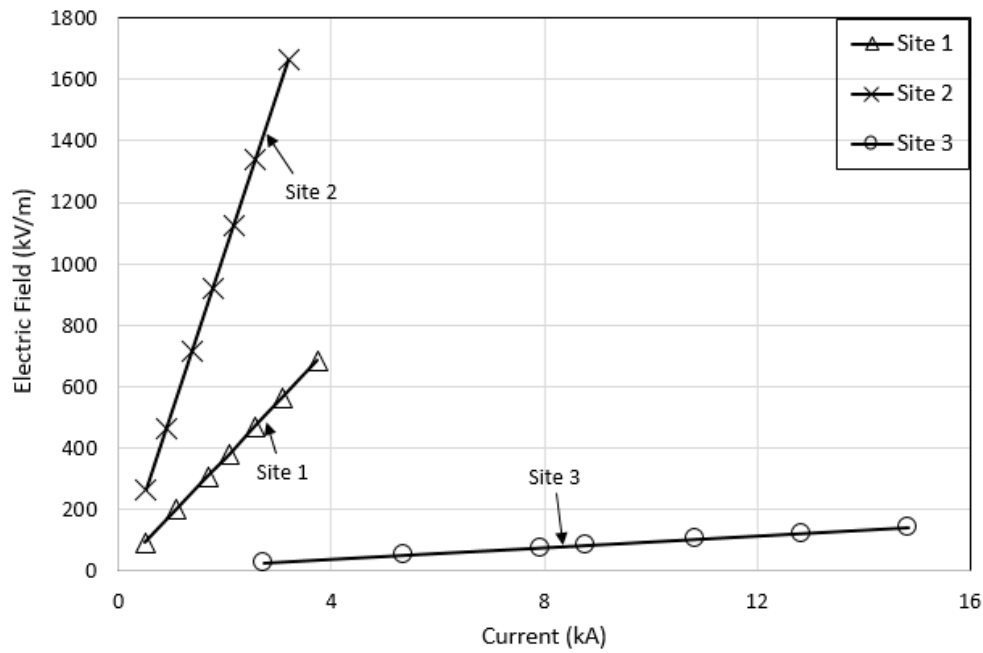
Figure 48. Highest electric field values at strip conductor versus applied current, for configuration 5, installed at various sites.
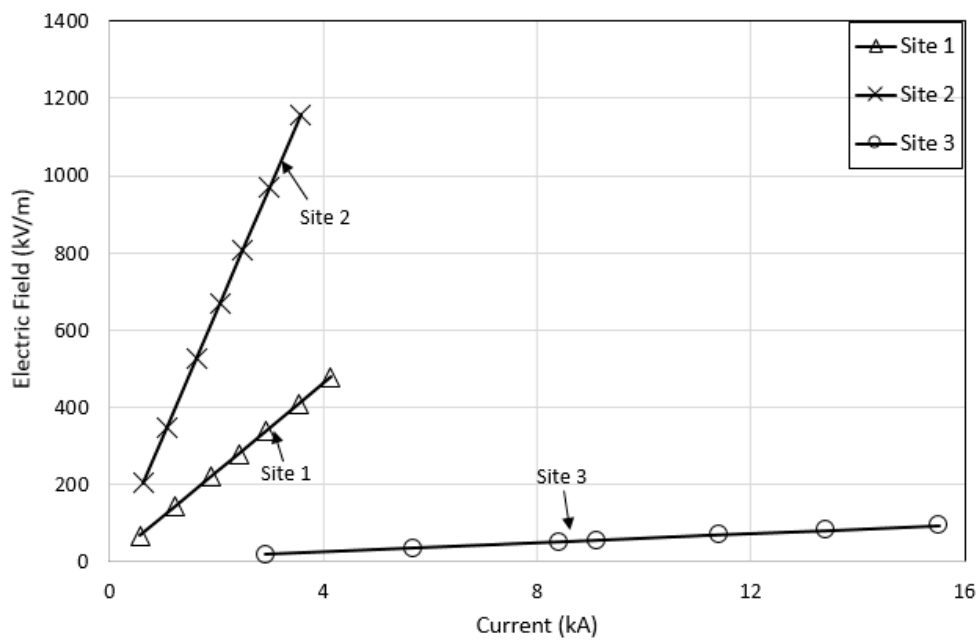
Figure 49. Highest electric field values at strip conductor versus applied current, for configuration 6, installed at various sites.

In this study, FEM is performed to determine the electric field for various configurations, and soil resistivity values, which may not be achieved by experimental work. As is generally known, for the ionization process to occur, electric field value will have to exceed the critical electric field value of the grounding system. Thus, it would be expected that the ionization process would occur in grounding systems with a high electric field. The finding in this paper, from FEM simulation, found that the highest electric field values are seen for configurations at site 2. These observations again support the experimental results, where the high non-linearity, or reduction in ground impedance values, is significant for grounding systems with high electric field (i.e., configurations at sites 1 and 2), and the smallest electric field values are noticed for configurations at site 3, where $Z_{impulse}$ for configurations

at site 3 are almost constant, independent of current magnitudes due to its smaller electric field value, in comparison to other configurations installed at other sites. Table 12 summarises the results of different ground electrode configurations and soil resistivity on the computed electric field values.
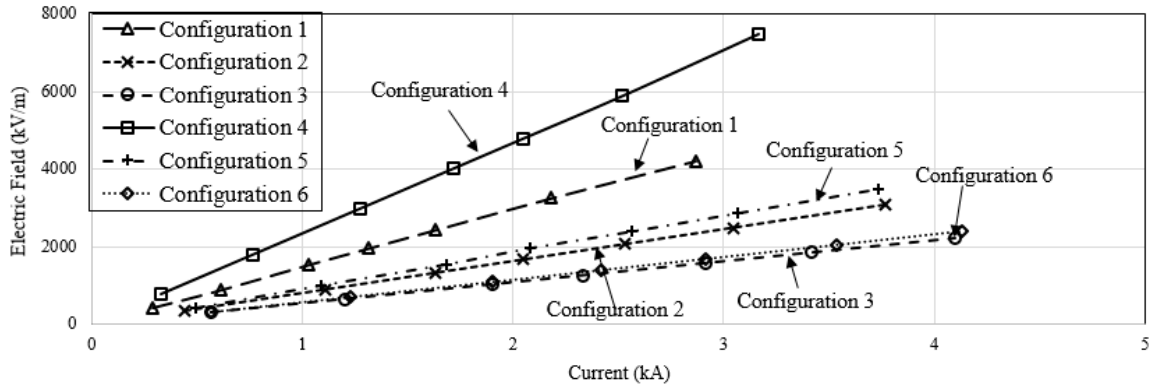
Figure 50. Highest electric field values at rod electrode versus applied current for all configurations, installed at site 1.
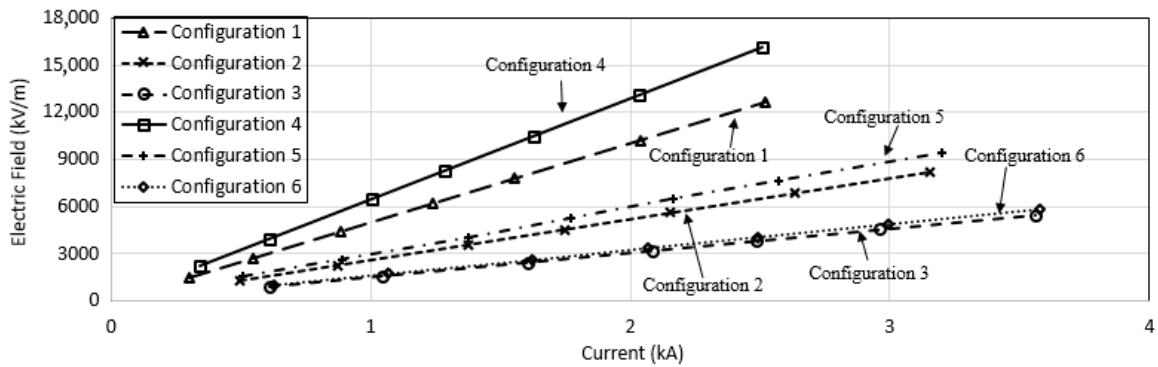
Figure 51. Highest electric field values at rod electrode versus applied current for all configurations, installed at site 2.
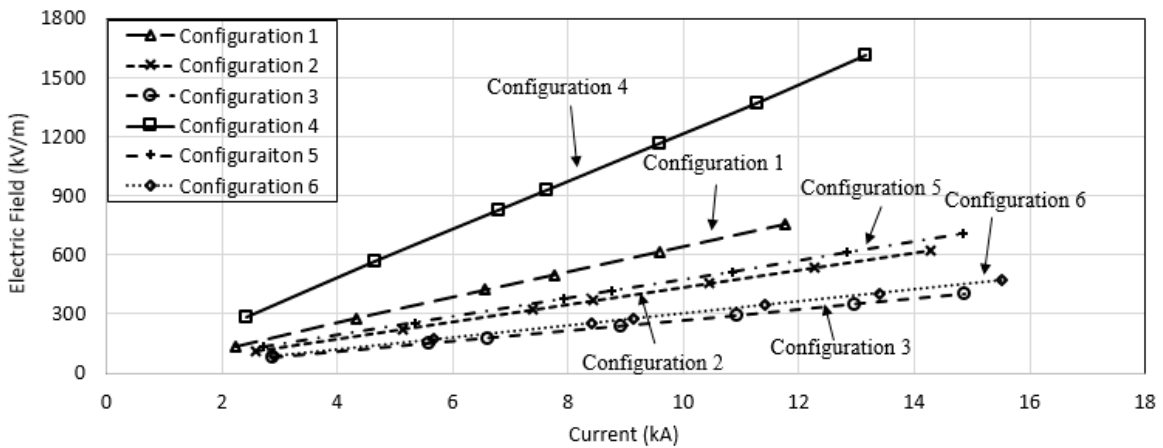
Figure 52. Highest electric field values at rod electrode versus applied current for all configurations, installed at site 3.

Table 12. Summary of the Effect of Soil Resistivity and Electrode Configuration on the Electric Field Values at Rod and Strip Electrodes.

Configuration	Electric Field Values for Various Configurations
1	
2	Electric field values increase with increasing current magnitudes for all configurations,
3	with the highest electric field occurring at the rod electrodes.
4	
5	For all sites, configuration 4 has the highest electric field, followed by configuration 1.
6	The largest difference in electric field is seen between configuration 1 and 4, in comparison
2	to configuration 2 and 5, and 3 and 6.
3	For the same configuration, site 2 has the highest electric field, and a steep increase with
4	increasing current magnitudes, with site 3 having the smallest electric field, with a small
5	increase in electric field with increasing current magnitudes, for all configurations.
6	

5. Conclusions

The effects of earth electrode configuration and soil resistivity on current rise time, time taken for current to discharge to ground and $Z_{impulse}$ are investigated experimentally at field sites, using computational methods. Six configurations of earth electrodes installed at various sites are tested both at steady-state and under high impulse conditions. It has been observed that a significant reduction in Rdc is found in site 3 (low soil resistivity), when a conventional electrode is replaced with a GDSR.

When subjected under high impulse conditions, it is established that the time to peak current decreases with voltage magnitudes. However, faster time to peak current is seen for configurations installed at site 2 (high soil resistivity), than those at site 1. This is thought to be due to the larger number of air voids in high resistivity soil (site 2), thus providing faster growth of ionization, as seen in some publications. In addition, it is also observed that most earth electrodes with low Rdc have faster discharging times due to the relatively low value of the resistance, compared to high Rdc. The time for current to discharge to zero, which provides an indication of the effectiveness of the grounding systems in discharging high current to the ground, is also analysed. It is discovered that there is a slower time for current to discharge to zero for grounding systems with high soil resistivity, and high Rdc.

When $Z_{impulse}$ with increasing currents are plotted, it is found that $Z_{impulse}$ values are dependent on current magnitudes for configuration 1, and become weak dependent on current magnitudes for grounding systems with lower Rdc. Higher $Z_{impulse}$ is also observed for the grounding systems with high Rdc. On the other hand, when FEM is performed for all the grounding systems using the current magnitudes obtained from experimental data, it is found that there is a higher electric field in electrode configurations installed at site 2 (high resistivity soil). For configurations installed at site 3 (low soil resistivity), low electric field values are achieved independently of current magnitudes. Large differences in computed electric field values at the rod electrode and copper strip are seen between configuration 1 and 4, and the smallest difference is seen between configurations 3 and 6 (large grounding configurations).

References

1. IEEE. *IEEE Standard 142: 2007—IEEE Recommended Practice for Grounding of Industrial and Commercial Power Systems*; IEEE: Piscataway, NJ, USA, 2007.
2. BSI. *BS 7430-1998, 'Earthing', British Standard Code of Practice*; BSI: London, UK, 2013.
3. IEEE. *IEEE Std 80-2013, IEEE Guide for Safety in AC Substation Grounding*; IEEE: Piscataway, NJ, USA, 2013.
4. IEEE. *IEEE Std 81-2012, IEEE Guide for Measuring Earth Resistivity, Ground Impedance, and Earth Surface Potentials of a Ground System*; IEEE: Piscataway, NJ, USA, 2012.
5. Abdul Ali, A.; Ahmad, N.; Mohamad Nor, N.; Reffin, M.; Syed Abdullah, S. Investigations on the performance of a new grounding device with spike rods under high magnitude current conditions. *Energies* **2019**, *12*, 1138. [CrossRef]
6. Yunus, S.; Mohamad Nor, N.; Agbor, N.; Abdullah, S.; Ramar, K. Performance of earthing systems for different earth electrode configurations. *IEEE Trans. Ind Appl.* **2015**, *51*, 5335–5342. [CrossRef]
7. Reffin, M.S.; Mohamad Nor, N.; Ahmad, N.N.; Abdullah, S.A. Performance of practical grounding systems under high impulse conditions. *Energies* **2018**, *11*, 3187. [CrossRef]
8. Reffin, M.; Ali, A.; Mohamad Nor, N.; Ahmad, N.; Abdullah, S.; Mahmud, A.; Hanaffi, F. Seasonal influences on impulse characteristics of grounding system for tropical countries. *Energies* **2019**, *12*, 1334. [CrossRef]
9. Haddad, A.; Griffiths, H.; Ahmeda, M.; Harid, N. Experimental investigation of the impulse characteristics of practical ground electrode systems. In Proceedings of the International Conference on High Voltage Engineering and Application (ICHVE), New Orleans, LA, USA, 11–14 October 2010; pp. 469–472.
10. Sonoda, T.; Takesue, H.; Sekioka, S. Measurement on surge characteristics of grounding resistance of counterpoises for impulse currents. In Proceedings of the 25th International Conference on Lightning Protection, Rhodes, Greece, 18–22 September 2000; pp. 411–415.
11. Sekioka, S.; Hayashida, H.; Hara, T.; Ametani, A. Measurement of grounding resistance for high impulse currents. *IEE Proc. Generat. Transm. Distrib.* **1998**, *145*, 693–699. [CrossRef]
12. Yang, S.; Zhou, W.; Huang, J.; Yu, J. Investigation on impulse characteristic of full-scale grounding grid in substation. *IEEE Trans. Electromagn. Compat.* **2018**, *60*, 1993–2001. [CrossRef]
13. Guo, D.; Clark, D.; Lathi, D.; Harid, N.; Griffiths, H.; Ainsley, A.; Haddad, A. Controlled large-scale tests of practical grounding electrodes—Part II: Comparison of analytical and numerical predictions with experimental results. *IEEE Trans. Power Del.* **2014**, *29*, 1240–1248. [CrossRef]
14. Stojkovic, Z.; Savic, M.S.; Nahman, J.M.; Salamon, D.; Bukorovic, B. Sensitivity analysis of experimentally determined grounding grid impulse characteristics. *IEEE Trans. Power App. Syst.* **1998**, *13*, 1136–1141. [CrossRef]
15. Elzowawi, A.; Haddad, A.; Griffiths, H.; Clark, D. Investigation of soil ionization propagation in two-layer soil samples. In Proceedings of the 50th International Universities Power Engineering Conference (UPEC), Stoke-Upon-Trent, UK, 1–4 September 2015; pp. 1–5.
16. Visacro, S.; Alipio, R.; Murta Vale, M.H.; Pereira, C. The response grounding electrodes to lightning currents: The effect of frequency-dependent resistivity and permittivity of soil. *IEEE Trans. Power Del.* **2011**, *53*, 401–406. [CrossRef]
17. Visacro, S.; Alipio, R. Frequency dependence of soil parameters: Experimental results, predicting formula and influence on the lightning response of grounding electrodes. *IEEE Trans. Power Del.* **2012**, *27*, 927–935. [CrossRef]
18. Alipio, R.; Visacro, S. Impulse efficiency of grounding electrodes: Effect of frequency-dependent soil parameters. *IEEE Trans. Power Del.* **2014**, *29*, 716–723. [CrossRef]
19. CIGRE. *Impact of Soil-parameter Frequency Dependence on the Response of Grounding Electrodes and on the Lightning Performance of Electrical Systems*; Technical Brochure 781; CIGRE: Paris, France, 2019.
20. Current Distribution, Electromagnetic Interference, Grounding and Soil Structure Analysis (CDEGS) Manual. Available online: https://www.sestech.com/common/distro_docs/16.0/PDF/GetStart.pdf (accessed on 25 February 2020).
21. Telekom Malaysia Berhad and Multimedia Unviersity. Experiment and Equipment Arrangement (Set Up) For Grounding Assessment under High Impulse Conditions. MALAYSIA—Patent Application No. Pl 2020002177, 30 April 2020.

22. Mohamad Nor, N.; Haddad, A.; Griffiths, H. Characterisation of ionisation phenomena in soils under fast impulses. *IEEE Trans. Power Del.* **2006**, *21*, 353–361.

23. Snowden, D.P.; Erler, J.W. Initiation of electrical breakdown of soil by water vaporization. *IEEE Trans. Nucl. Sci.* **1983**, *30*, 4568–4571. [CrossRef]

24. Higazi, K.A.; Chalmers, J.A. Measurements of atmospheric electrical conductivity near the ground. *J. Atmos. Terr. Phys.* **1966**, *28*, 327–330. [CrossRef]

25. Srisakot, S.; Dana, G.; Mohamad Nor, N.; Griffiths, H.; Haddad, A. Effect of frequency on soil characteristics. In Proceedings of the 36th Universities Power Engineering Conference (UPEC), Swansea, UK, 12–14 September 2001; p. 156.

26. Harid, N.; Griffiths, H.; Haddad, A. Effect of ground Return path on impulse characteristics of earth electrodes. In Proceedings of the 7th Asia-Pacific International Conference on Lightning, Chengdu, China, 1–4 November 2011.